ETH zürich

Hydro-mechanical modeling of the earthquake cycle

Luca Dal Zilio

Effective normal stress

$$\tau = f\,(\sigma - p)$$

Shear stress

Friction
(Rate-and-state)

Normal stress

Pore pressure

1. Modeling variation in pore pressure due to poroelastic bulk (1 example)

2. Modeling fully coupled hydro-mechanical coupling (2 examples)

Faults are frequently not isolated structures but act as integral components of a broader network of geological fractures that can interplay through stress fields (Scholz and Gupta, 2000).

Earthquakes that occur in the setting of intricate fault networks are capable of extending across multiple fault segments during significant events. For instance, the 2016 Mw 7.8 Kaikoura earthquake ruptured at least 21 segments of the Marlborough fault system (e.g., Ulrich et al., 2019).

Dynamic rupture model

Slip inversion

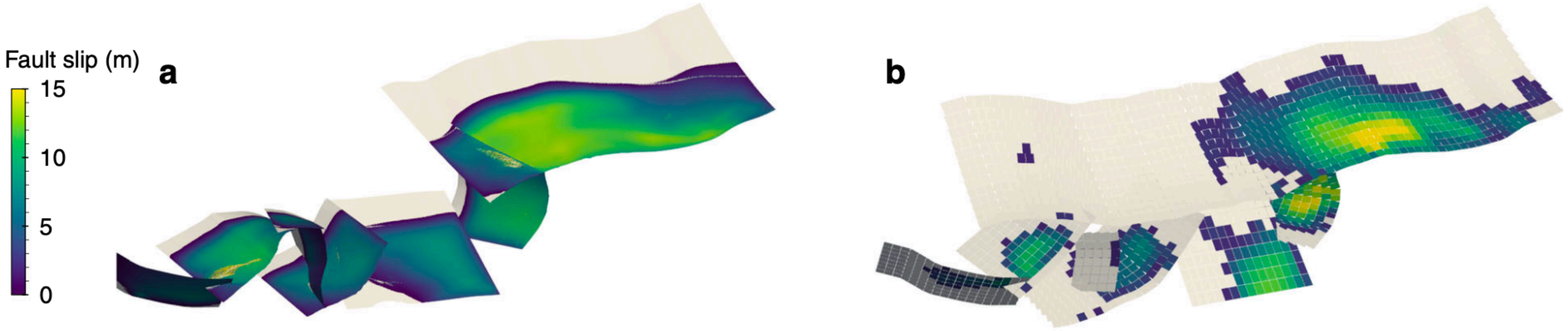

Ulrich, Gabriel, Ampuero, Xu (2019)

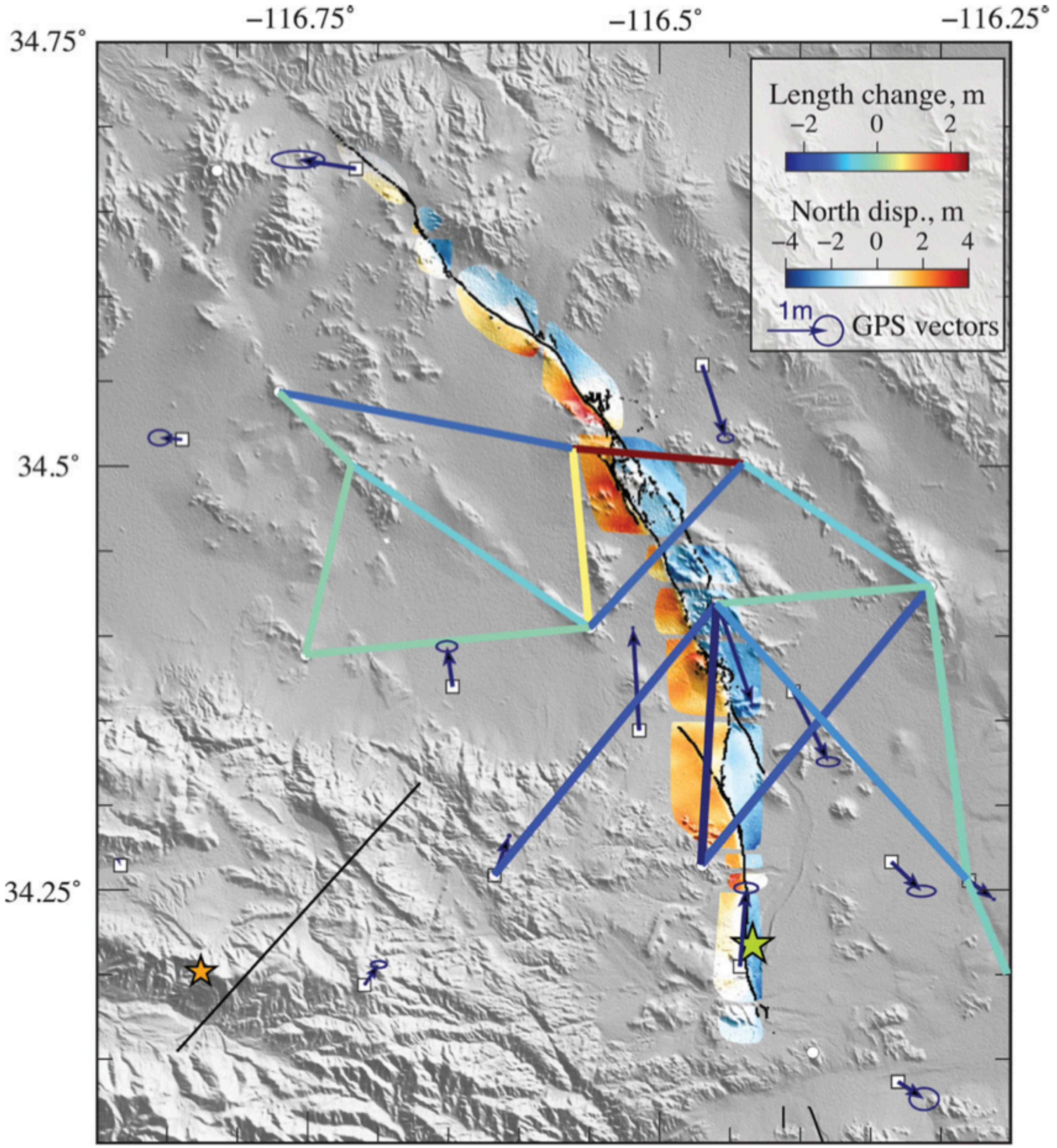

Gombert et al., (2018) and Sieh et al. (1993)

One such geometric complexity that may influence the rupture length is a **fault stepover** characterized by an arrangement of disjointed, parallel fault segments offset from each other at the Earth's surface.

The 1992 Landers earthquake is an ideal instance of such a scenario—it ruptured at least four fault segments exhibiting a right-stepping pattern to the north and generated a Mw 7.3 event (e.g., Sieh et al., 1993, and many others).

Predicted coseismic pore-pressure change at 0.5 km depth during the magnitude-6.5 earthquake in the south Iceland seismic zone

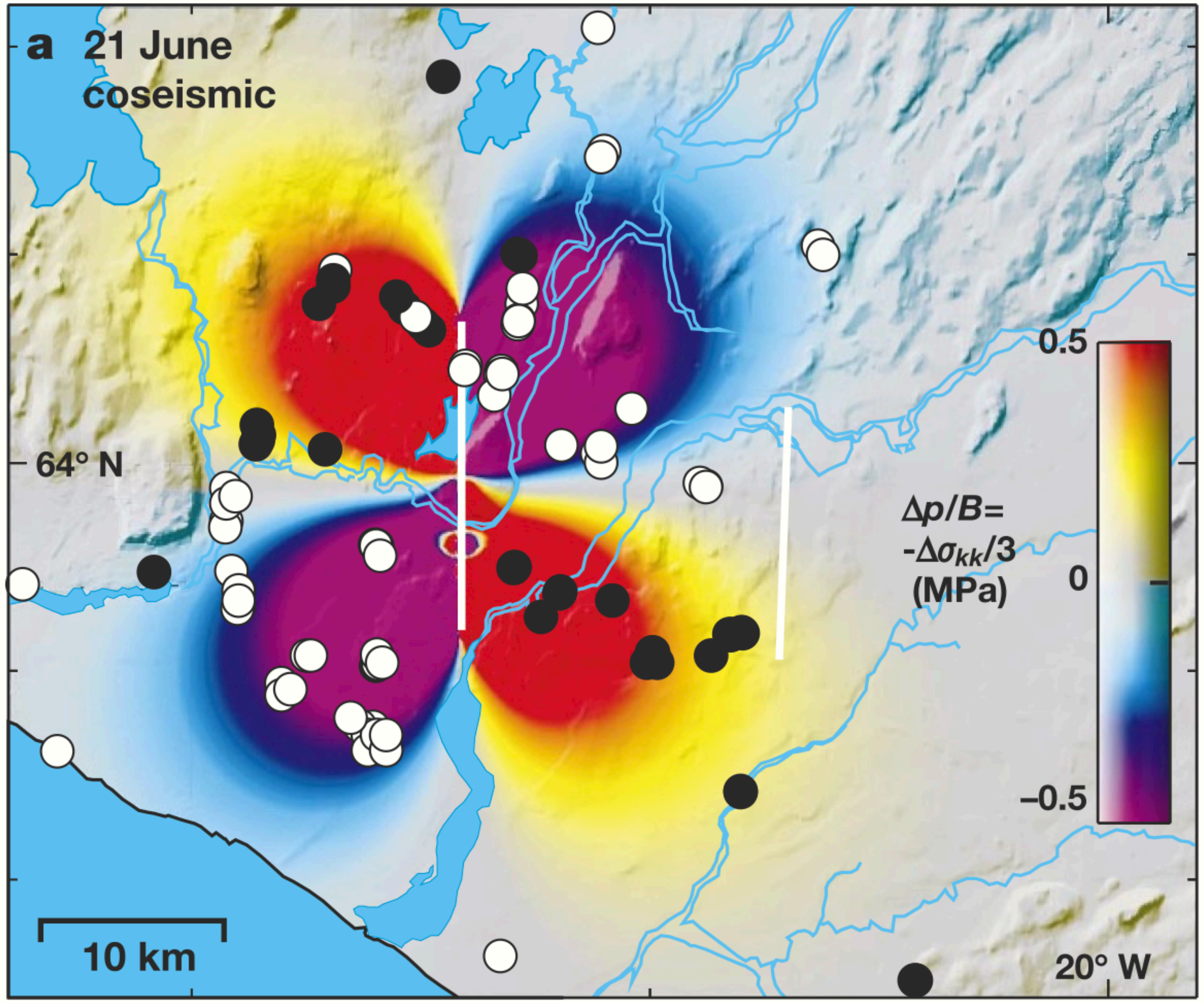

Jónsson, Segall, Pedersen, Björnsson (2000)

Large earthquakes alter the stress in the surrounding crust. A number of time-dependent processes, including afterslip, pore-fluid flow and viscous relaxation of the lower crust and upper mantle, further modify the stress and pore pressure near the fault during earthquakes.

The capacity of multiple fault segments to rupture simultaneously within a single earthquake event is essential to improving our knowledge of the potential upper limits of earthquake magnitudes since seismic moments increase in proportion to the ruptured area.

Predicted coseismic pore-pressure change at 0.5 km depth during the magnitude-6.5 earthquake in the south Iceland seismic zone

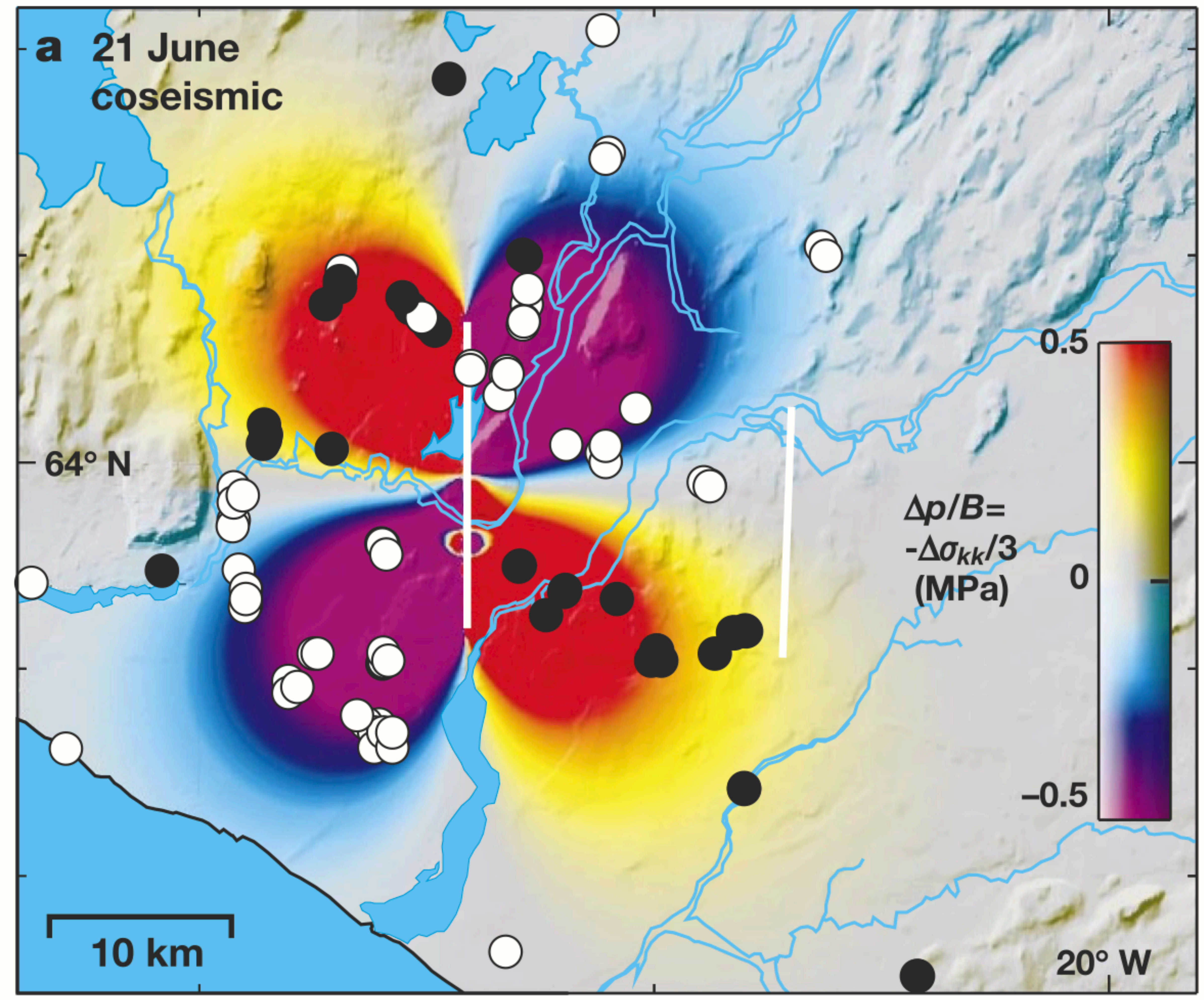

Jónsson, Segall, Pedersen, Björnsson (2000)

Do earthquake-triggered poroelastic effects influence neighboring faults?

* not to scale

How does poroelasticity influence the dynamic rupture to jump across fault stepovers?

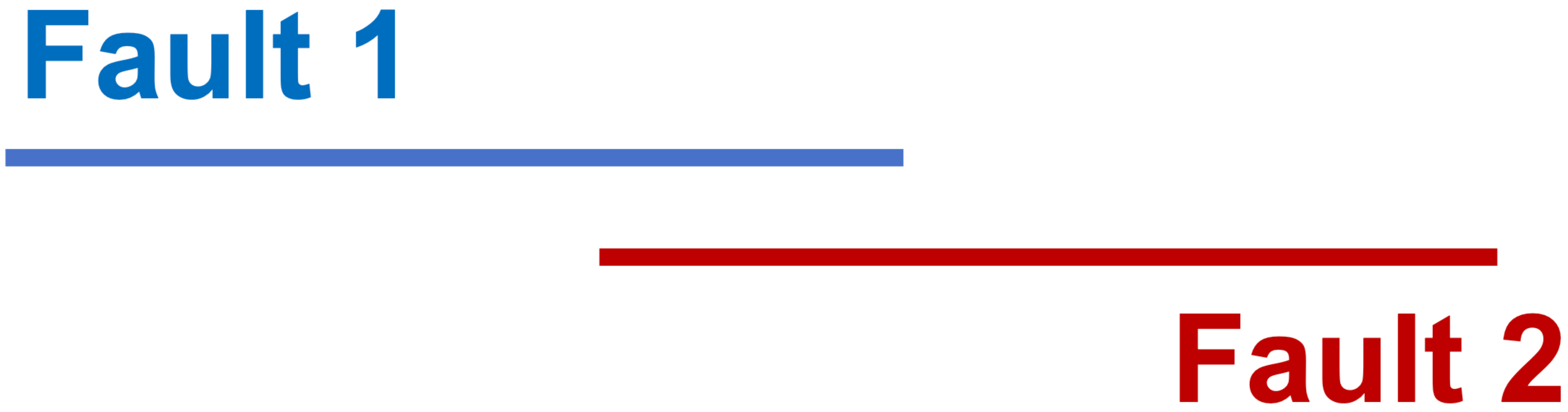

* not to scale

Dynamics of Fault Interaction: Parallel Strike-Slip Faults

RUTH A. HARRIS

U.S. Geological Survey, Menlo Park, California

STEVEN M. DAY

Department of Geological Sciences, San Diego State University, San Diego, California

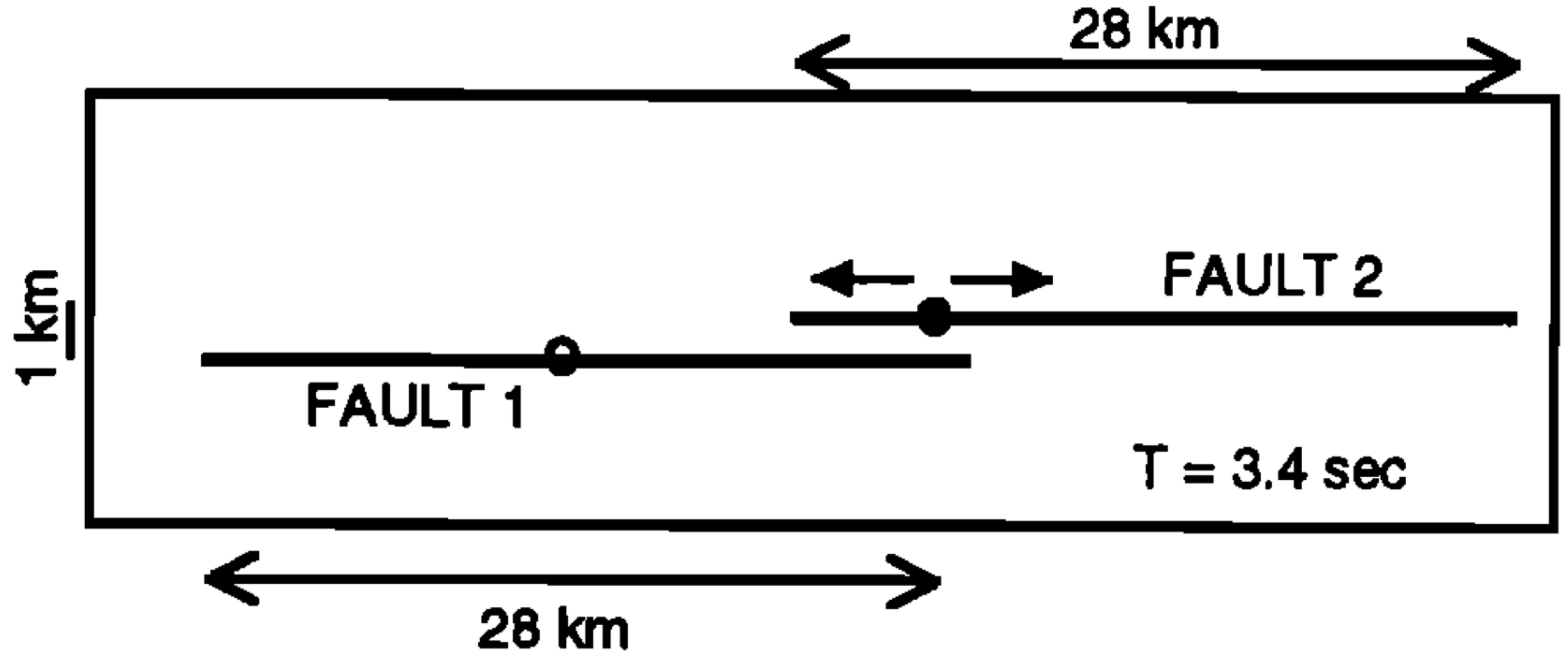

Slip-weakening Fracture Criterion

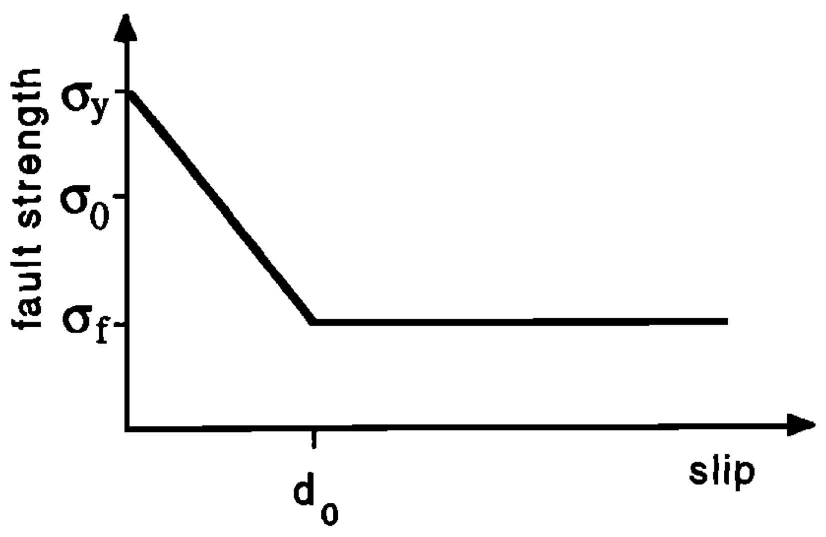

PROCEDURE

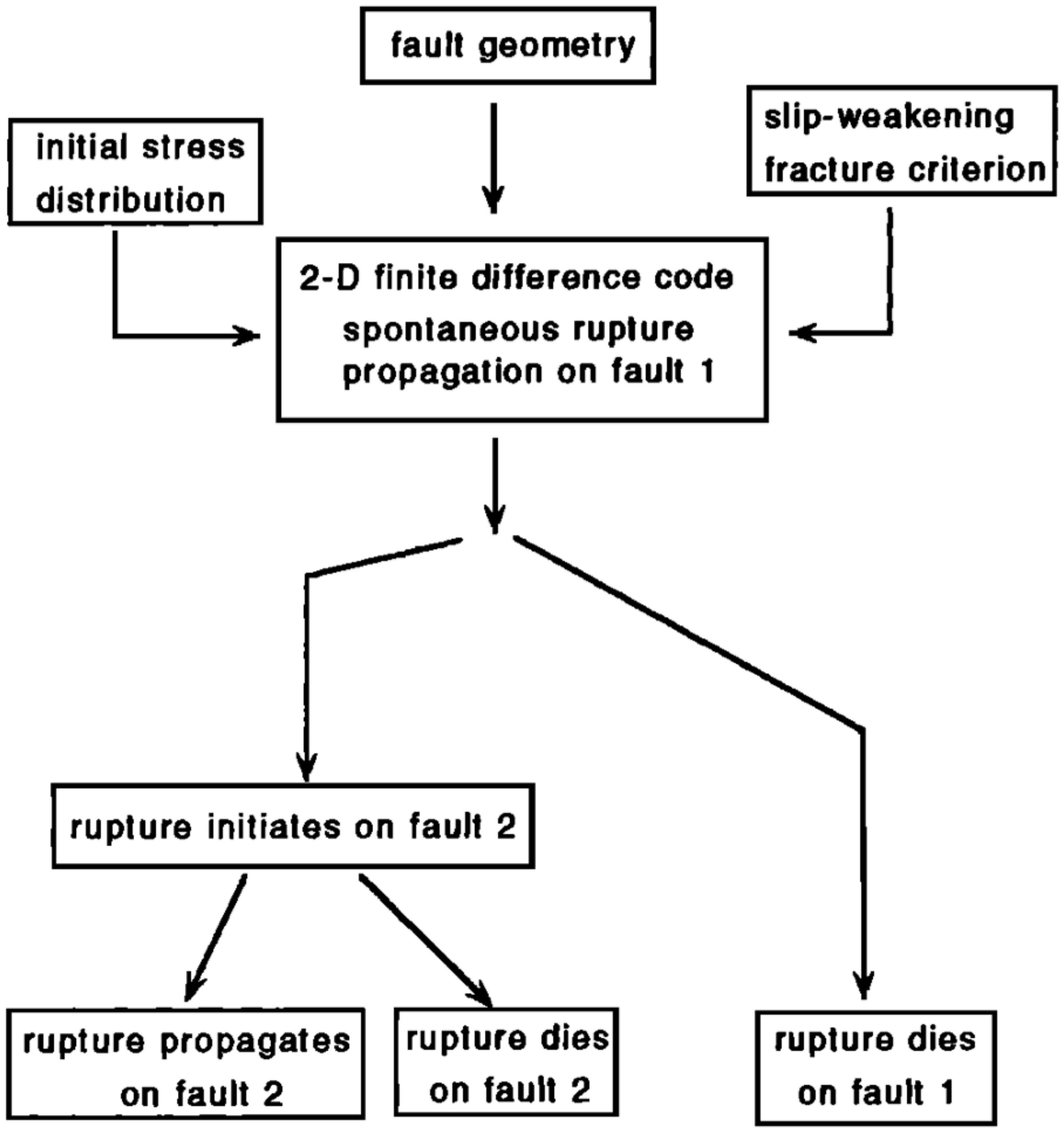

How does poroelasticity influence the dynamic rupture to jump across fault stepovers over multiple seismic cycles?

To address this question, we introduce a quasi-dynamic Boundary Element Model that simulates 2D plane-strain earthquake sequences.

$$\underbrace{\tau_0 + f(\delta(x,t)) - \frac{\mu}{2c_s}V}_{\textit{Elastodynamic shear stress}} = \underbrace{f\,(\sigma - p)}_{\textit{Shear resistance}}$$

$$\tau = f\,\overline{\sigma} = f_* + a\,ln\left(\frac{V}{V_*}\right) + b\,ln\left(\frac{\theta V}{D_{RS}}\right)\overline{\sigma}$$

$$\frac{d\theta}{dt} = 1 - \frac{V\theta}{D_{RS}}$$

Huang, Heimisson, Dal Zilio (2023, in prep.)

This model incorporates undrained pore pressure responses affecting the fault's clamping and unclamping.

$$\overline{\sigma} = (\sigma - \Delta p)$$

$$\Delta p = B\Delta\sigma_{kk}/3$$

$\Delta\sigma_{kk}/3$ ⟶ Time-dependent change in mean stress

$\Delta p = -B[(1+\nu_u)/3] + (\Delta\sigma_{xx} + \Delta\sigma_{zz})$ ⟶ Plain-strain assumption

Rice and Cleary (1976)

Harris and Day (1993)

The investigation of how poroelasticity influences the likelihood of an earthquake jumping through a stepover emerges as a significant area of study.

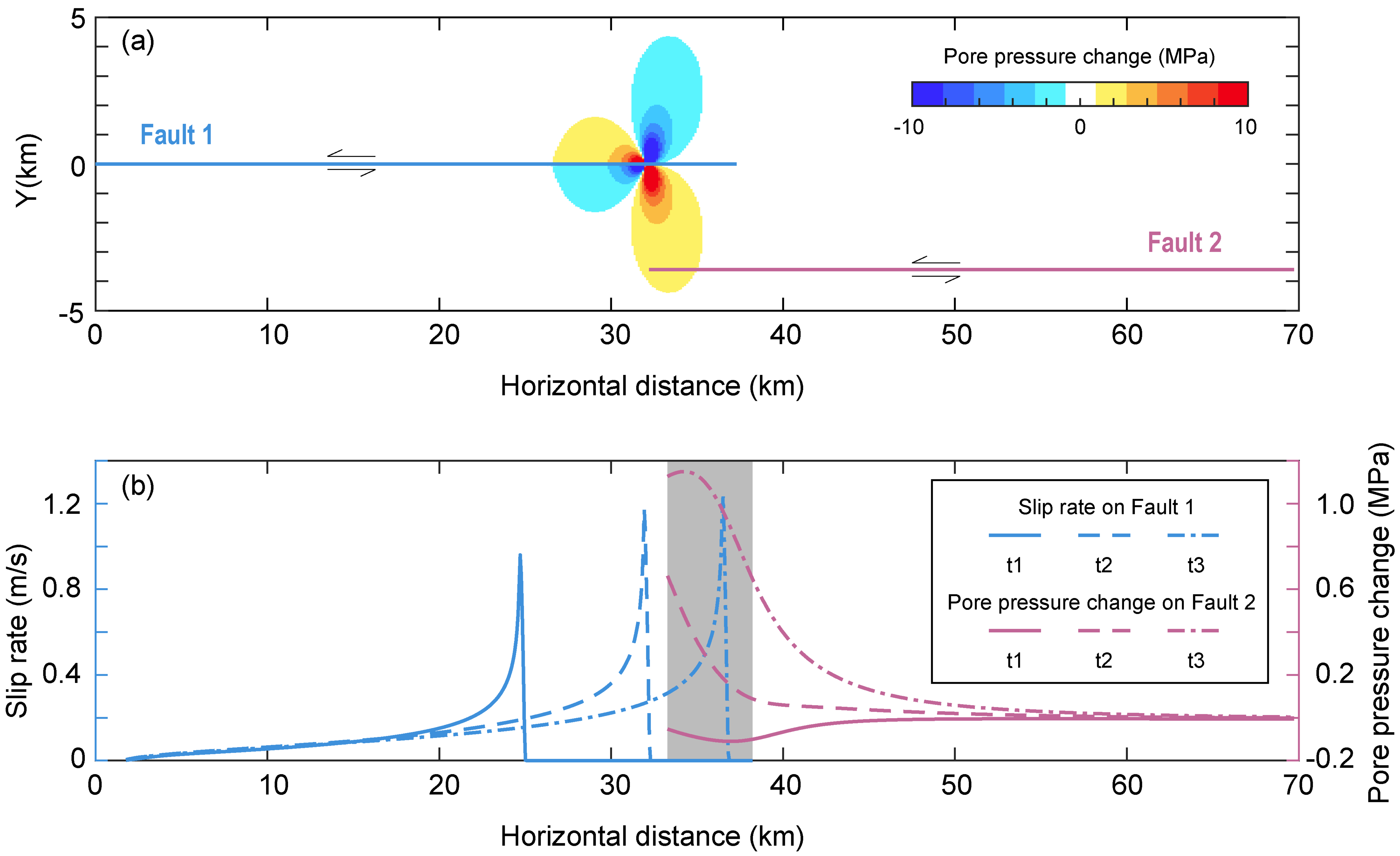

In-plane slipping along the fault leads to compaction on one side and dilatation on the other. As a result, there is an instantaneous response in slip-driven pore pressure, which can produce (un)clamping effects.

Huang, Heimisson, Dal Zilio (2023, in prep.)

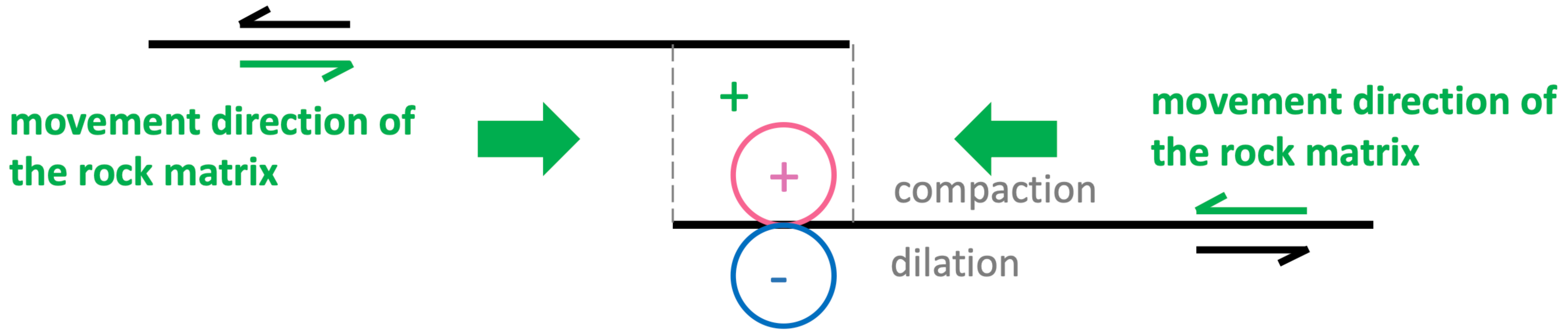

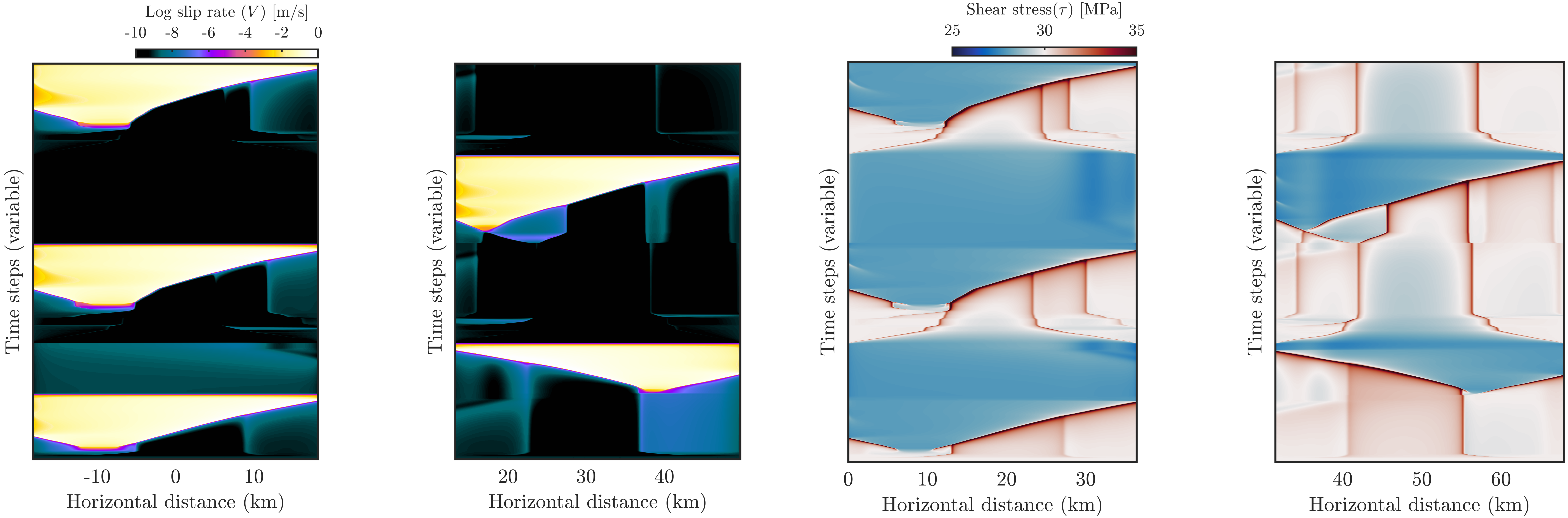

Huang, Heimisson, Dal Zilio (2023, in prep.)

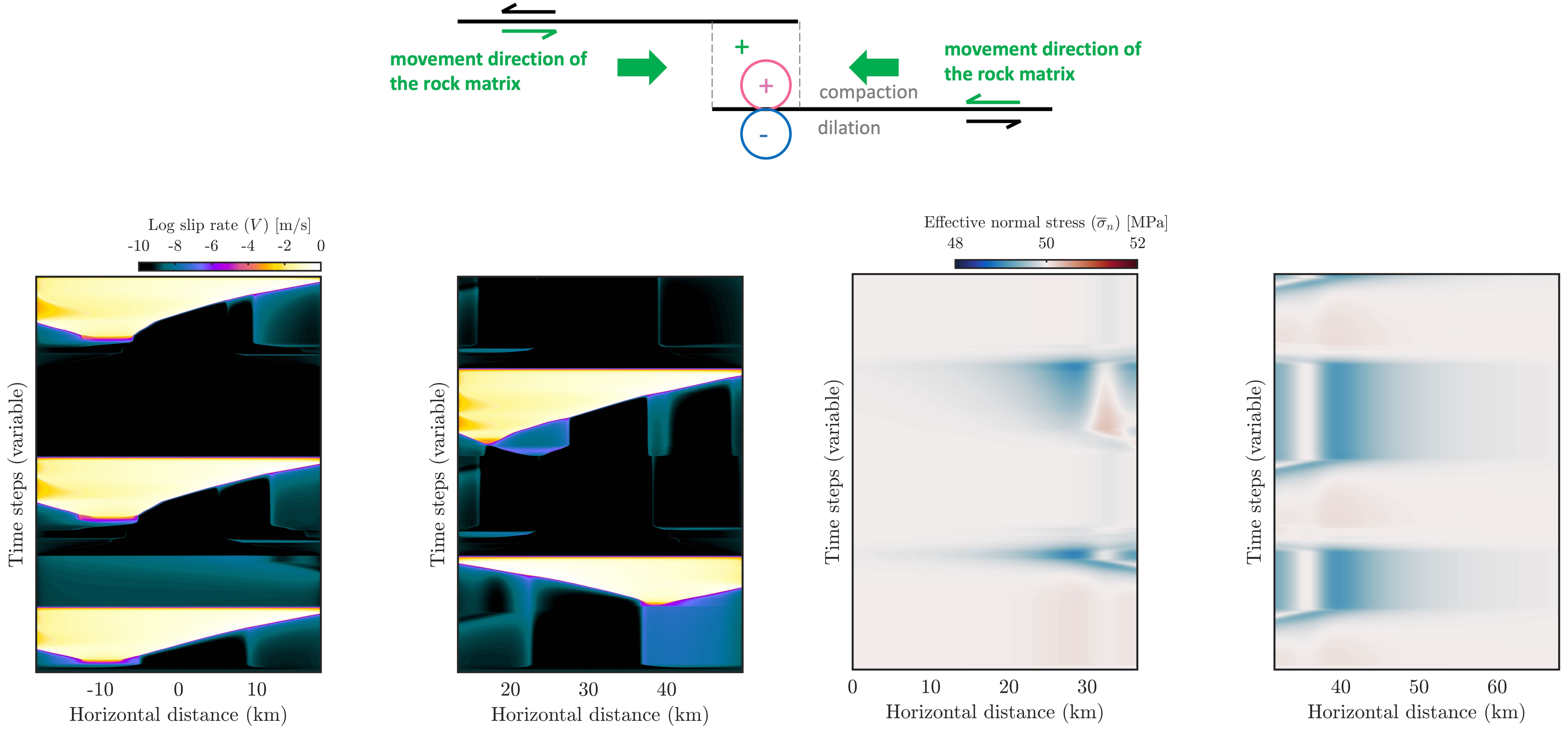

Huang, Heimisson, Dal Zilio (2023, in prep.)

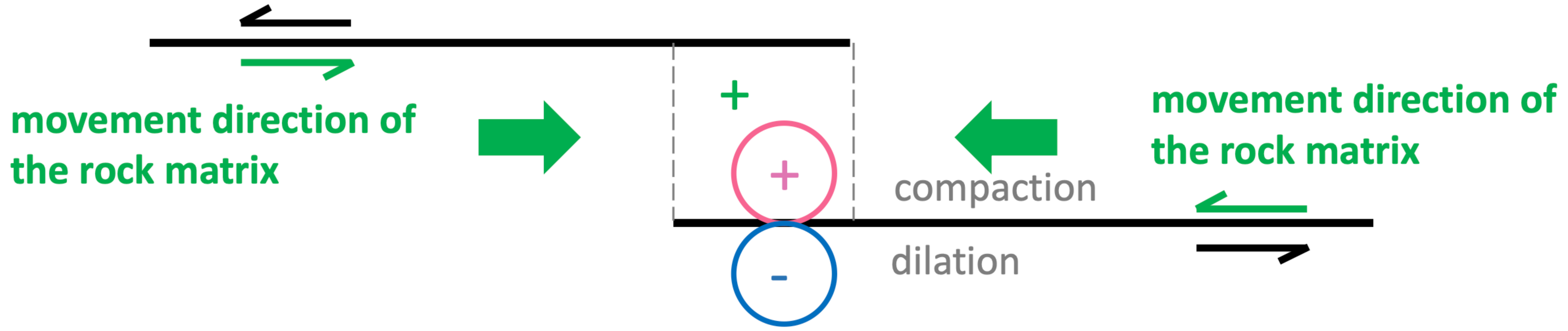

Competing mechanisms:

$$h^* = \frac{2}{\pi} \frac{\mu^* D_{RS}\, b}{\overline{\sigma}\, (b-a)^2};$$

Huang, Heimisson, Dal Zilio (2023, in prep.)

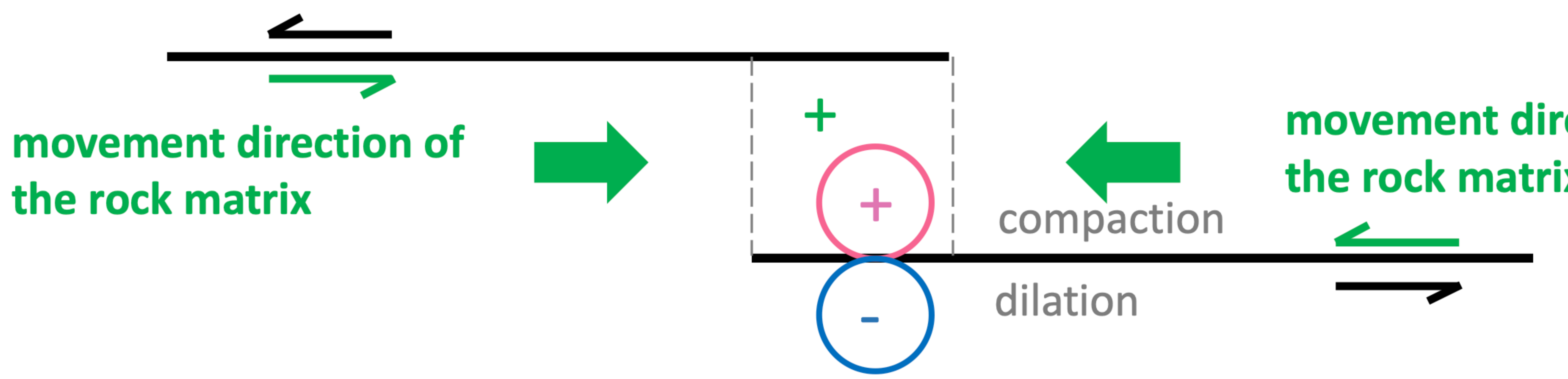

$$h^* = \frac{2}{\pi} \frac{\mu^* D_{RS}\, b}{\overline{\sigma}\,(b-a)^2};$$

Competing mechanisms:

1. Increase of the effective normal stress: clamping effect and smaller nucleation size

2. Decrease of the effective normal stress: unclamping effect and larger nucleation size

Huang, Heimisson, Dal Zilio (2023, in prep.)

B=0.4

B=1.0

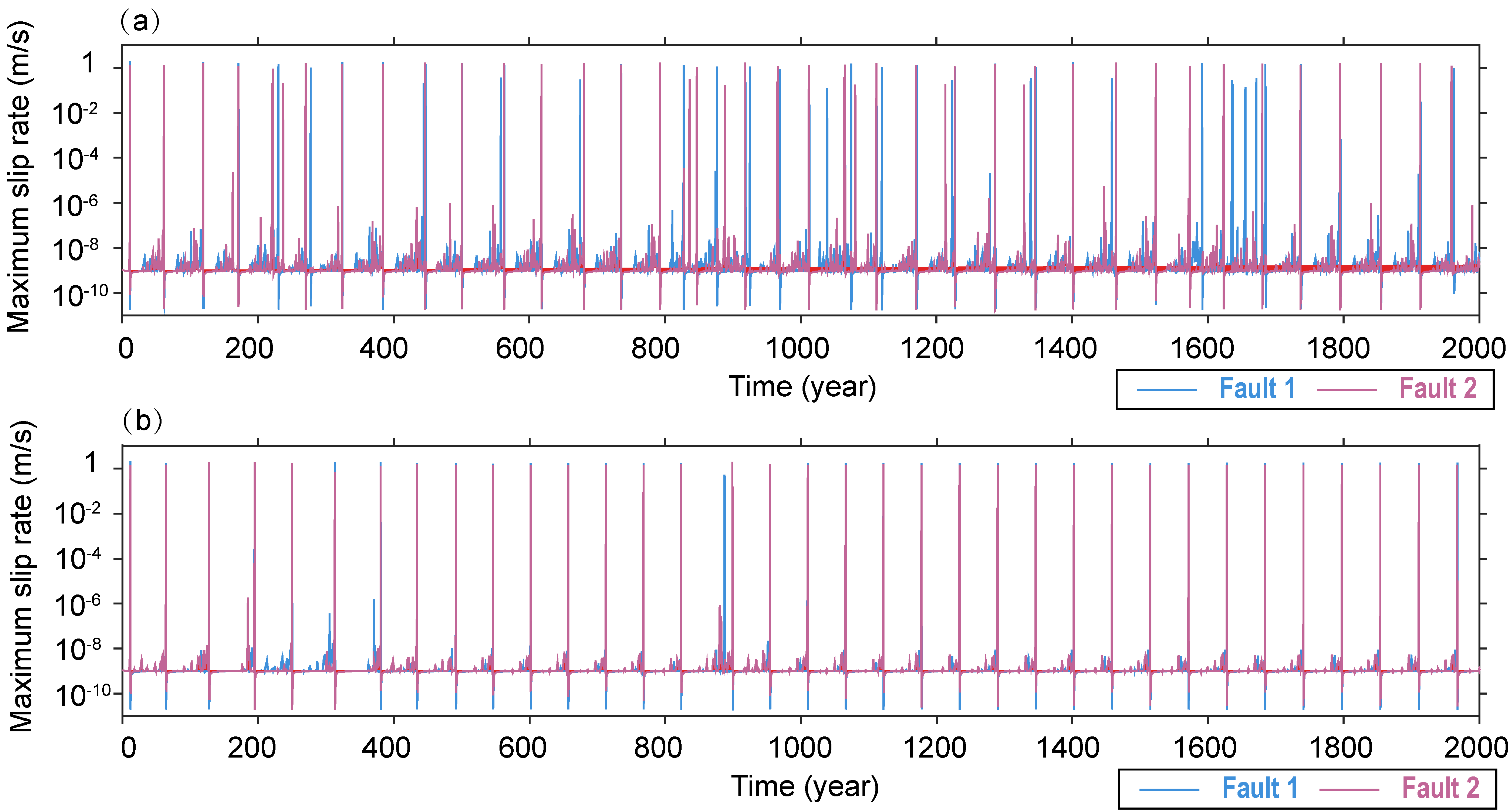

Huang, Heimisson, Dal Zilio (2023, in prep.)

Impact of poroelastic effects on rupture jumping probability, assuming different Skempton coefficients.

These results show how the evolution of stress (and pore-fluid pressure) on/off-fault can affect the seismic pattern over several seismic cycles.

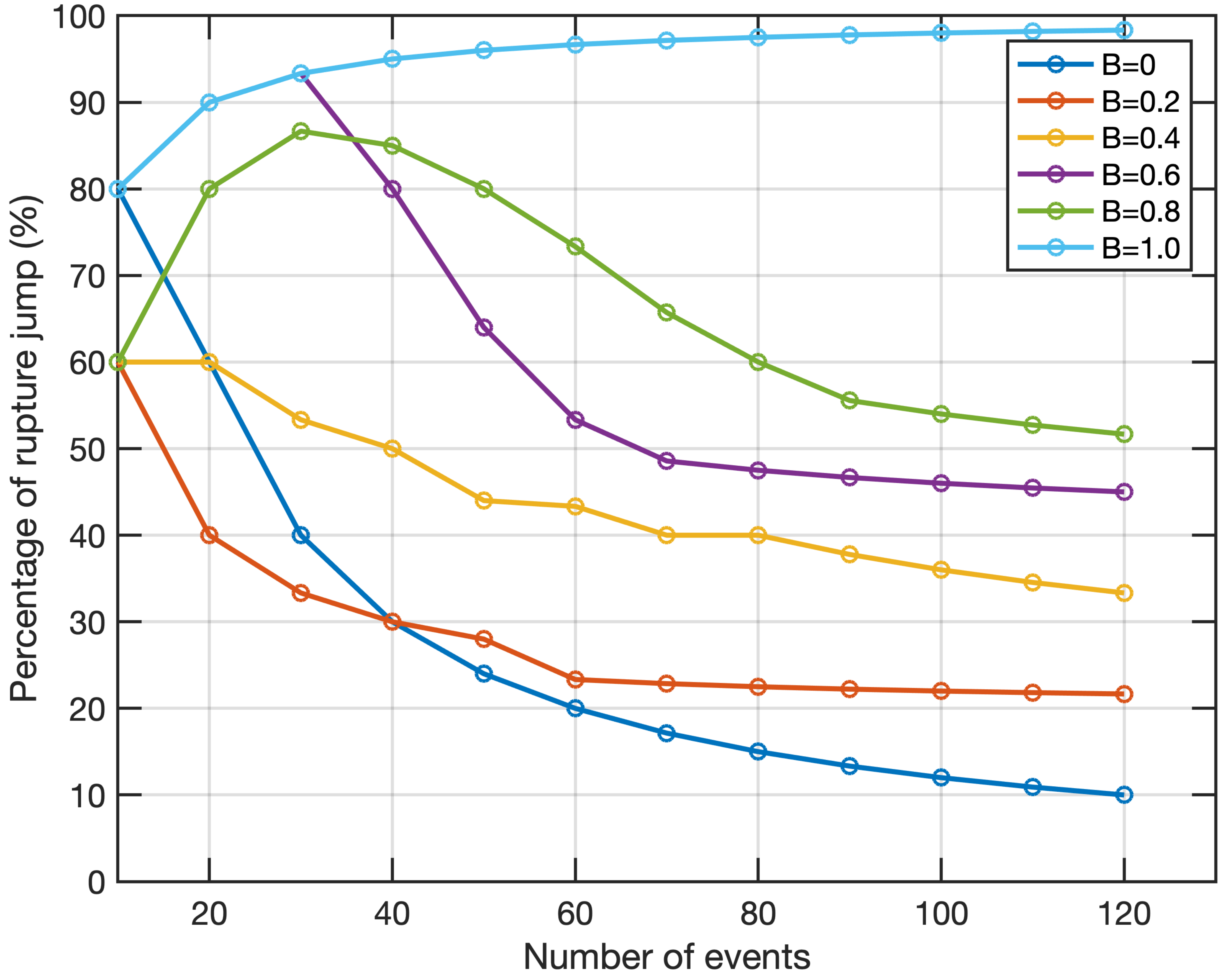

Huang, Heimisson, Dal Zilio (2023, in prep.)

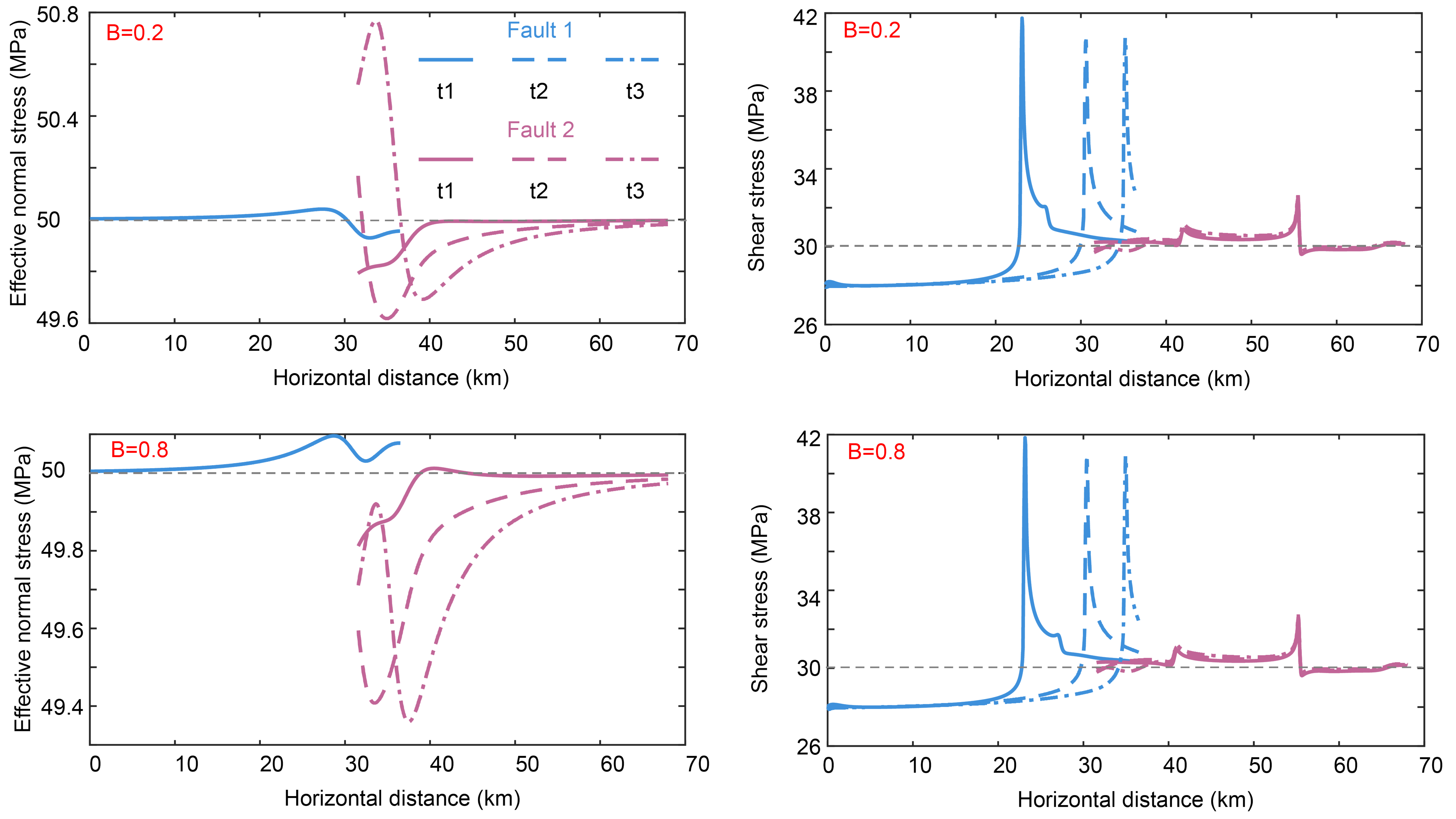

Huang, Heimisson, Dal Zilio (2023, in prep.)

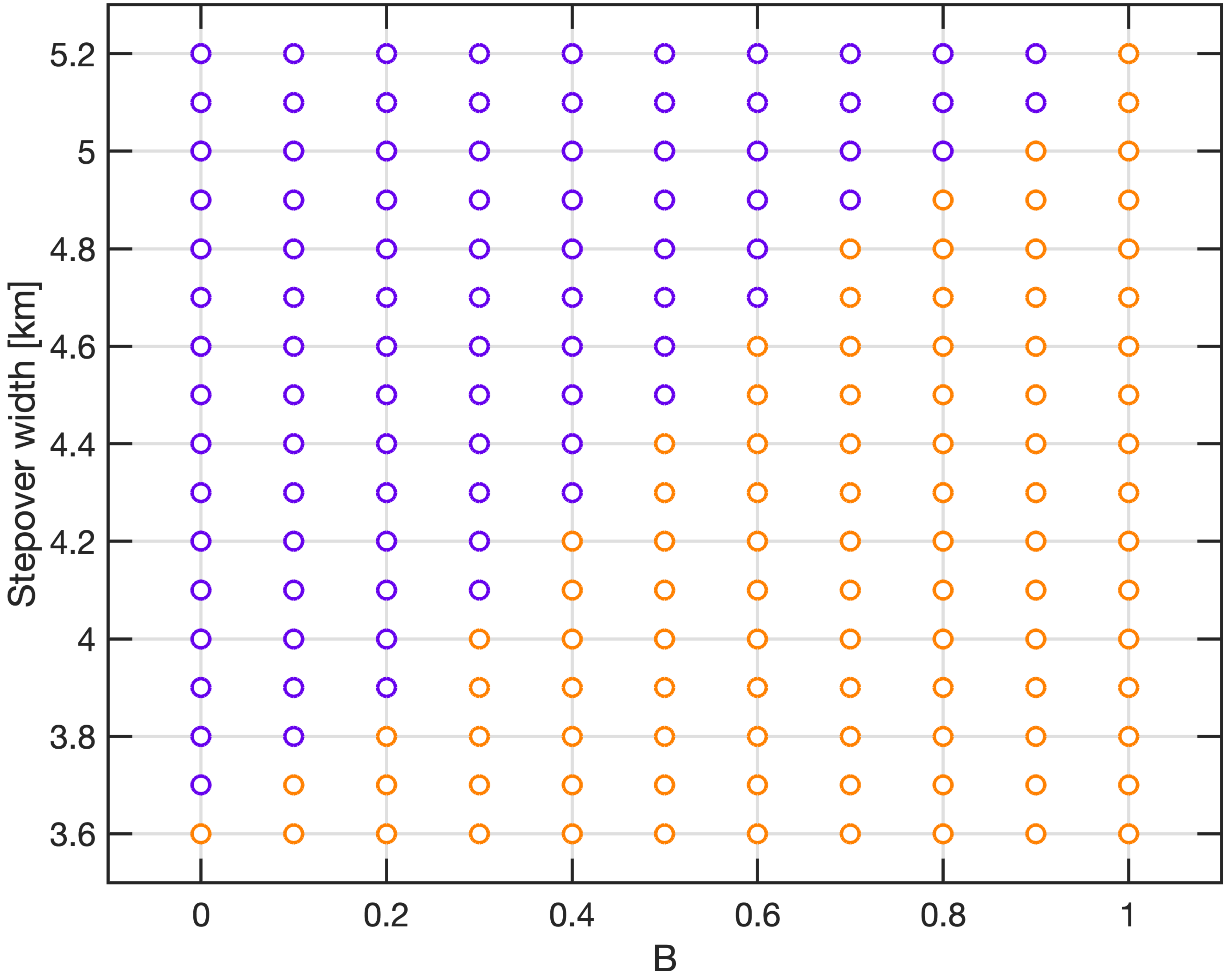

By testing a broad range of Skempton coefficients, we can determine the critical stepover width resulting in ≥50% of ruptures jumping to the second fault.

Huang, Heimisson, Dal Zilio (2023, in prep.)

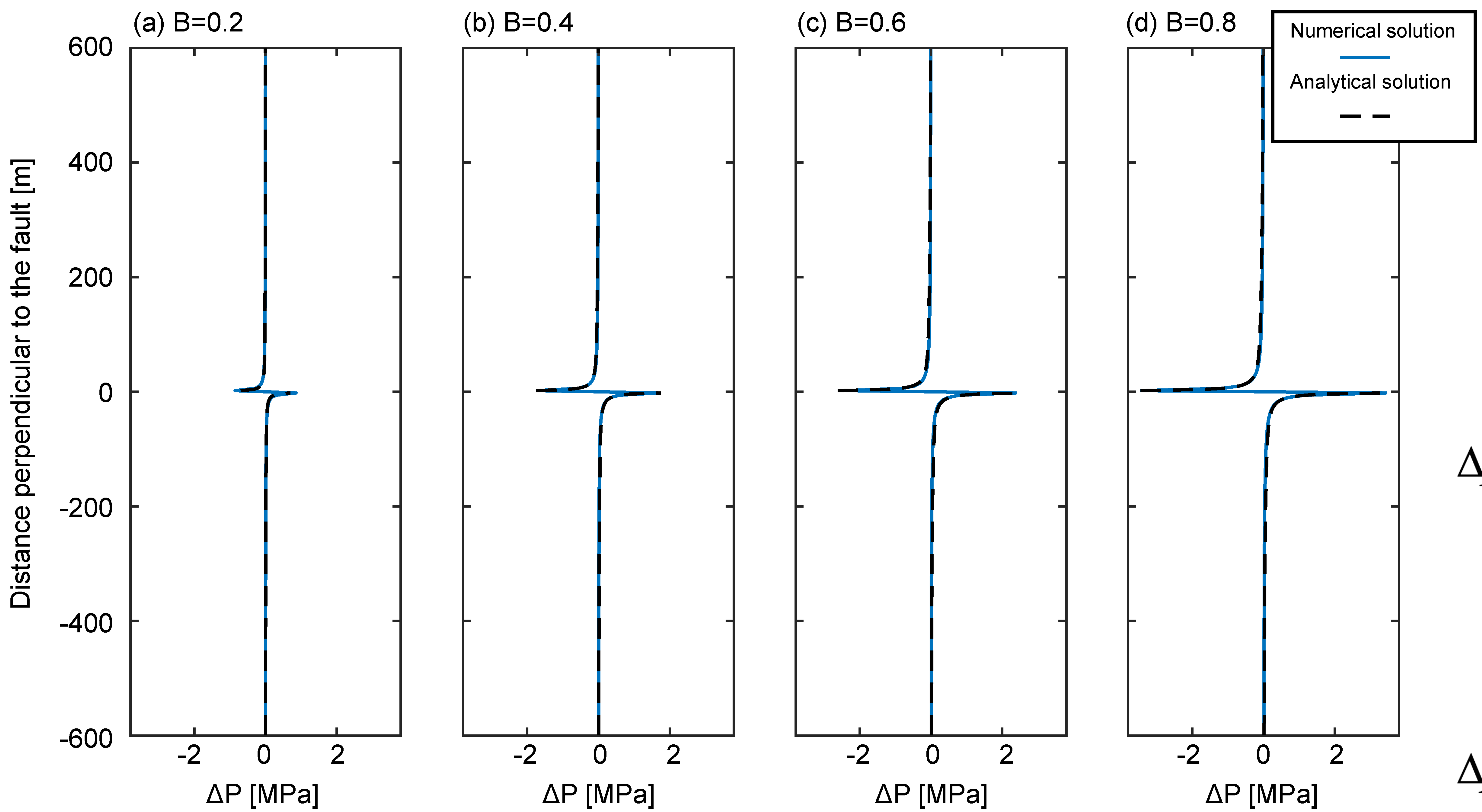

D: Dislocation
μ : a ratio relating undrain Poisson ratio and Poisson ratio
G: shear modulus
y: coordinate
υ_μ : undrain Poisson ratio
r: represents the distance from the origin

Analytical Solution

$$\Delta p_{analytical} = \frac{D\mu G}{2\pi(1-\upsilon_\mu)\eta}\frac{y}{r^2}$$

Numerical Solution

$$\Delta p_{numerical} = -B \times \left[\frac{\Delta\sigma_{kk}(t)}{3}\right]$$

Huang, Heimisson, Dal Zilio (2023, in prep.)

- ✅ Fault friction
- ✅ Fault interactions
- ✅ Poroelastic effect
- ✅ Computationally fast

- ❌ (Poro)-visco-elastic compressible medium
- ❌ Drained/undrained response of the porous media
- ❌ Evolution of permeability and porosity
- ❌ Three-dimensional

Why do we need complex models?

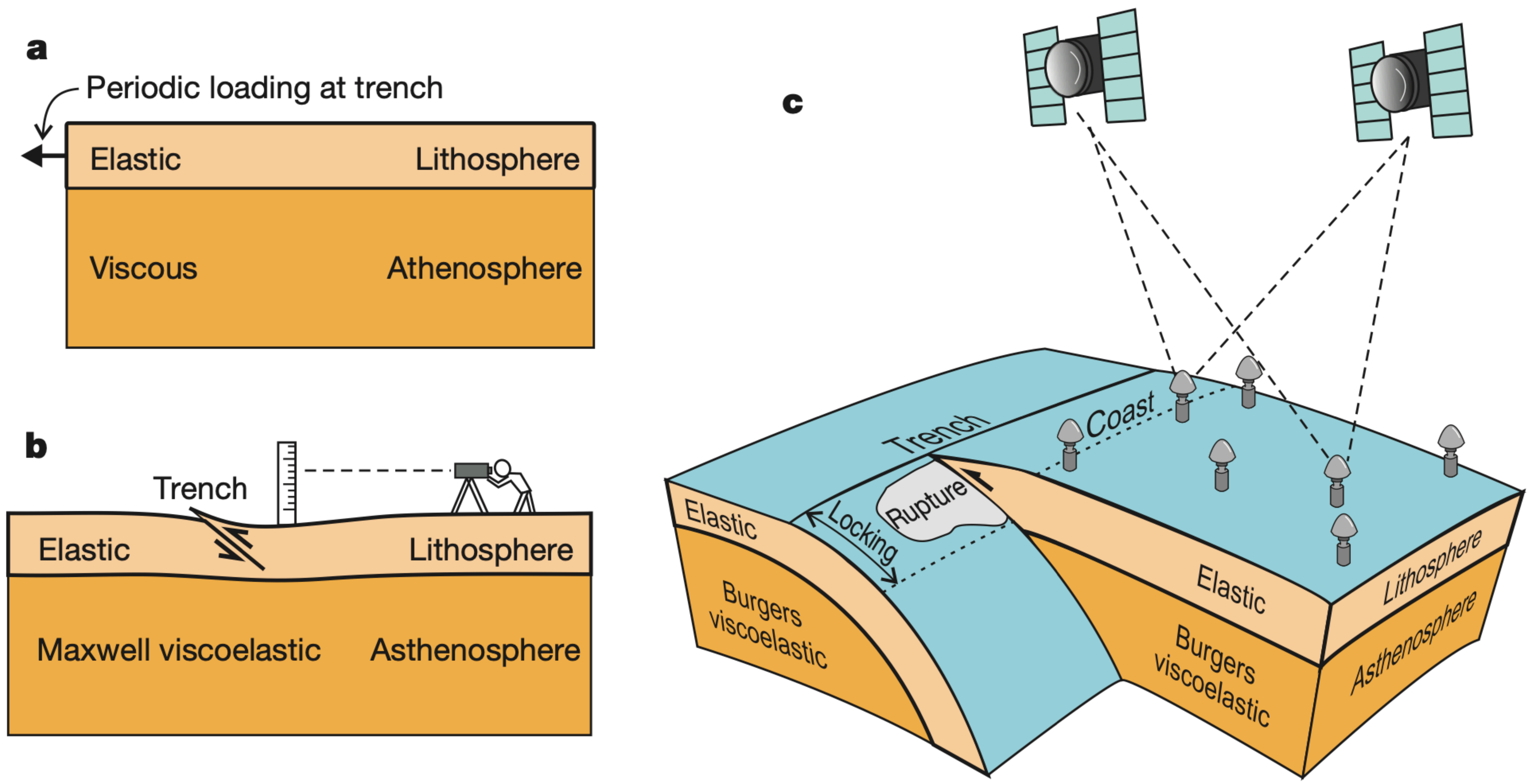

Wang, Hu, He (2012)

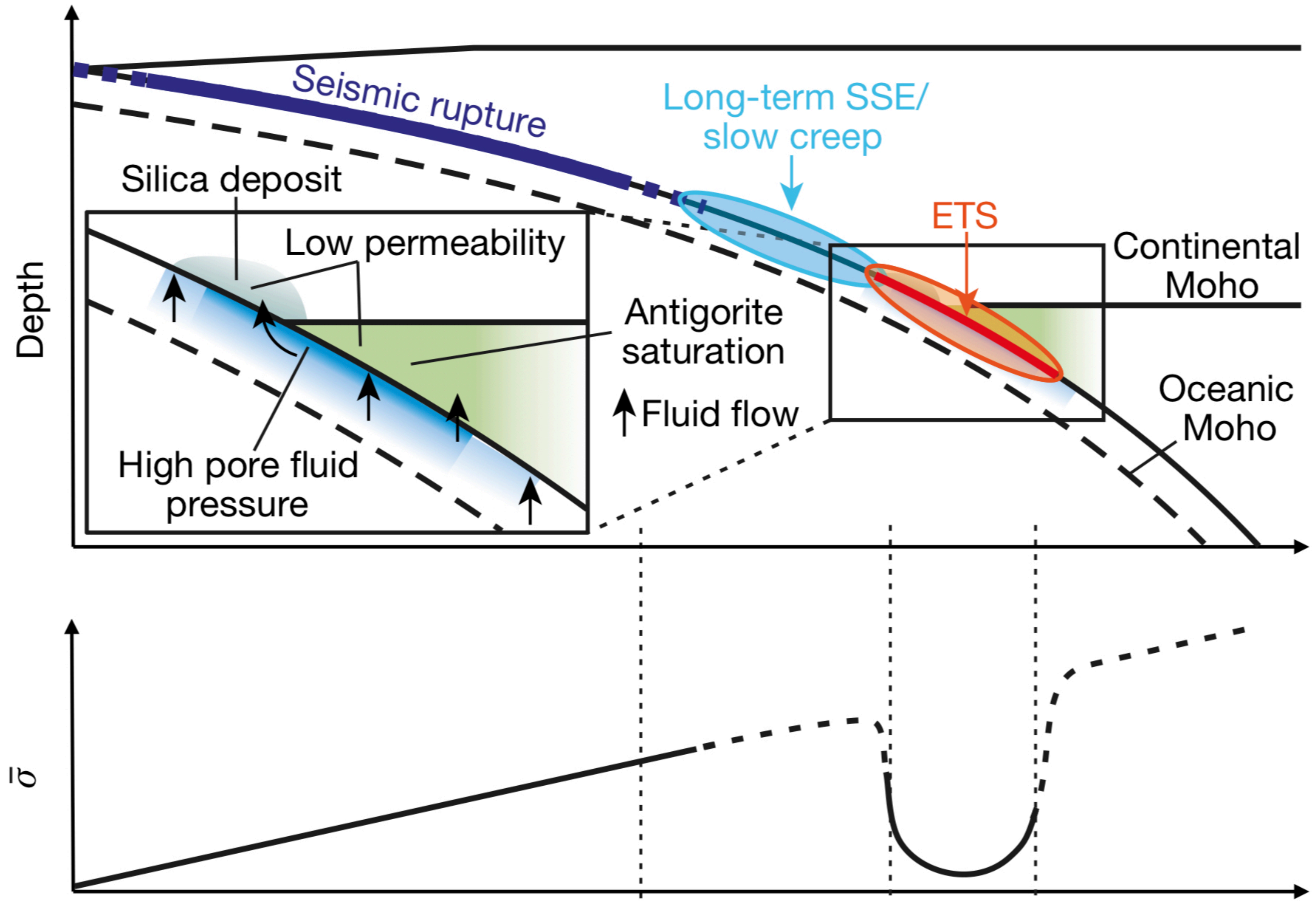

Gao and Wang (2017)

Slow-slip events and pore-fluid pressure cycling

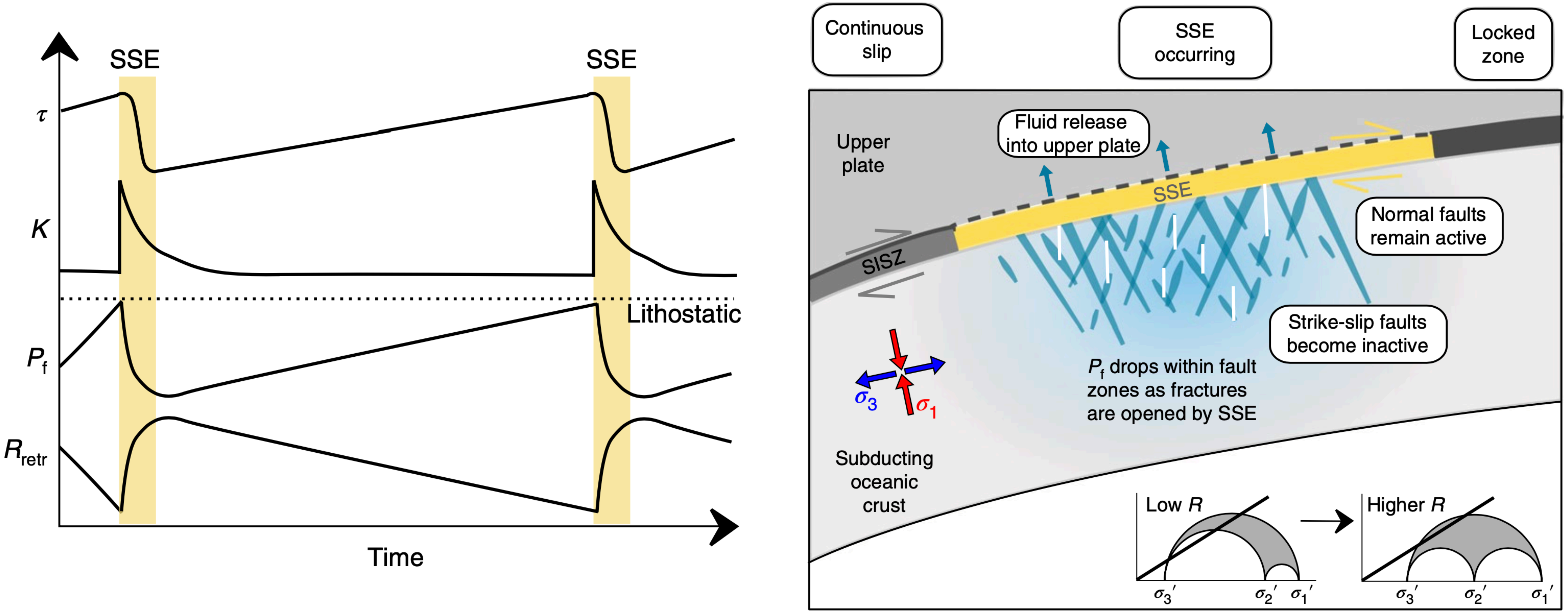

Warren-Smith et al., 2019

Recent observations using focal mechanisms **recorded on an ocean-bottom seismic network show temporal fluid pressure fluctuations through slow slip cycles.**

Hydro-Mechanical Earthquake Cycles (H-MECs)

2-D, continuum-based, finite difference code

Conservation equations for **total momentum** (solid matrix and fluid)

$$\nabla \cdot \underline{\underline{\boldsymbol{\sigma}}} + \boldsymbol{g}\,\rho^{[\mathrm{t}]} = \rho^{[\mathrm{t}]}\,\frac{D^{[\mathrm{s}]}\boldsymbol{v}^{[\mathrm{s}]}}{Dt}$$

Inertia term (fully dynamic)

$$\rho^{[\mathrm{t}]}\,\frac{D^{[\mathrm{s}]}\boldsymbol{v}^{[\mathrm{s}]}}{Dt} \approx (1-\phi)\,\rho^{[\mathrm{s}]}\,\frac{D^{[\mathrm{s}]}\boldsymbol{v}^{[\mathrm{s}]}}{Dt} + \phi\,\rho^{[\mathrm{f}]}\,\frac{D^{[\mathrm{f}]}\boldsymbol{v}^{[\mathrm{f}]}}{Dt}$$

We neglect the differences in the acceleration of solid and fluid.

$[\mathrm{s}]$ solid

$[\mathrm{f}]$ fluid

$[\mathrm{t}]$ total

Dal Zilio et al., 2022

Hydro-Mechanical Earthquake Cycles (H-MECs)

Fluid momentum

$$\boldsymbol{v}^{[\mathrm{D}]} = -\frac{k^{[\phi]}}{\eta^{[\mathrm{f}]}} \left(\nabla p^{[\mathrm{f}]} - \rho^{[\mathrm{f}]} \left(\boldsymbol{g} - \frac{D^{[\mathrm{f}]}\boldsymbol{v}^{[\mathrm{f}]}}{Dt}\right)\right)$$

Fully compressible solid mass

$$\nabla \cdot \boldsymbol{v}^{[\mathrm{s}]} = -\frac{1}{K^{[\mathrm{d}]}} \left(\frac{D^{[\mathrm{s}]}p^{[\mathrm{t}]}}{Dt} - \alpha \frac{D^{[\mathrm{f}]}p^{[\mathrm{f}]}}{Dt}\right) - \frac{p^{[\mathrm{t}]} - p^{[\mathrm{f}]}}{\eta^{[\phi]}(1-\phi)}$$

Drained bulk modulus ($K^{[\mathrm{d}]}$)

Biot-Willis coefficient (α)

Compaction viscosity ($\eta^{[\phi]}$)

Fully compressible fluid mass

$$\nabla \cdot \boldsymbol{v}^{[\mathrm{D}]} = \frac{\alpha}{K^{[\mathrm{d}]}} \left(\frac{D^{[\mathrm{s}]}p^{[\mathrm{t}]}}{Dt} - \frac{1}{B} \frac{D^{[\mathrm{f}]}p^{[\mathrm{f}]}}{Dt}\right) + \frac{p^{[\mathrm{t}]} - p^{[\mathrm{f}]}}{\eta^{[\phi]}(1-\phi)}$$

Skempton coefficient (B)

Hydro-Mechanical Earthquake Cycles (H-MECs)

Maxwell visco-elasto-plasticity (V-E-P)

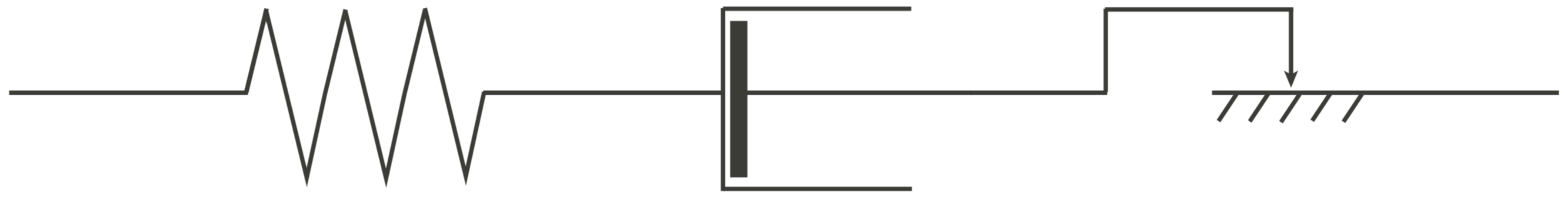

$$\dot{\varepsilon}'_{ij} = [\,\dot{\varepsilon}'_{ij}\,]_{\mathrm{viscous}} + [\,\dot{\varepsilon}'_{ij}\,]_{\mathrm{elastic}} + [\,\dot{\varepsilon}'_{ij}\,]_{\mathrm{plastic}}$$

$$[\,\dot{\varepsilon}'_{ij}\,]_{\mathrm{viscous}} = \frac{\tau_{ij}}{2\,\eta_{\mathrm{s}}} \qquad [\,\dot{\varepsilon}'_{ij}\,]_{\mathrm{elastic}} = \frac{1}{2\mu}\,\frac{\tilde{D}}{\tilde{D}t}\,(\tau_{ij}) \qquad [\,\dot{\varepsilon}'_{ij}\,]_{\mathrm{plastic}} = \chi\frac{\partial\tau_{ij}}{2\,\partial\tau_{II}}$$

Notably, in acontinuum approach the **physical quantities are invariant** of the coordinate system, which allows the solution to adapt to spontaneous bulk evolution. As such, we introduce an invariant formulation of the regularised version of RSF (Nakatani, 2001; Herrendörfer et al., 2018; Dal Zilio et al., 2022)

$$\tau = f\,\overline{\sigma} = f_* + a\,ln\left(\frac{V}{V_*}\right) + b\,ln\left(\frac{\theta V}{D_{RS}}\right)\overline{\sigma}$$

$$\tau = a\,\left(p^{[\mathrm{t}]} - p^{[\mathrm{f}]}\right)\,\mathrm{arcsinh}\left[\frac{V(t)}{2V_0}\exp\left(\frac{f_* + b\ln\left(\frac{\theta(t)V_0}{D_{RS}}\right)}{a}\right)\right]$$

* Regularized rate-and-state friction law

(e.g., Ben-Zion and Rice, 1997; Cochard and Madariaga, 1994; Crupi and Bizzarri, 2013; Dieterich, 1978, 1979; Lapusta et al., 2000; Rice and Ben-Zion, 1996; Rice, 1993; Ruina, 1983)

Model setup

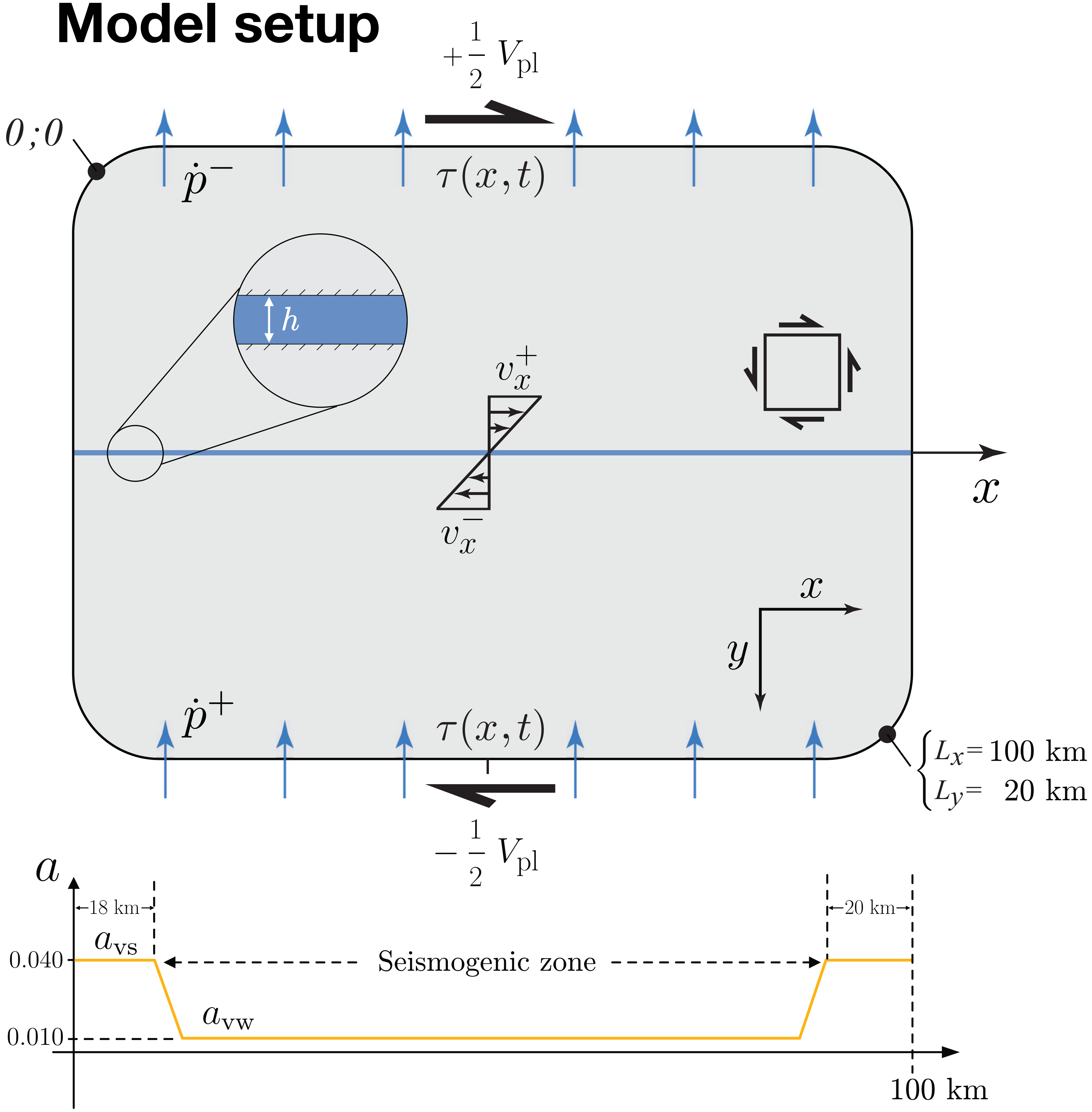

2D in-plane strike-slip setup loaded by constant velocity. We assume a fault with a finite thickness (h) and we impose an inward and outward flow from the lower and upper boundary.

The seismogenic region with velocity-weakening properties is surrounded by velocity-strengthening segments.

Sequences of fluid-driven seismic rupture

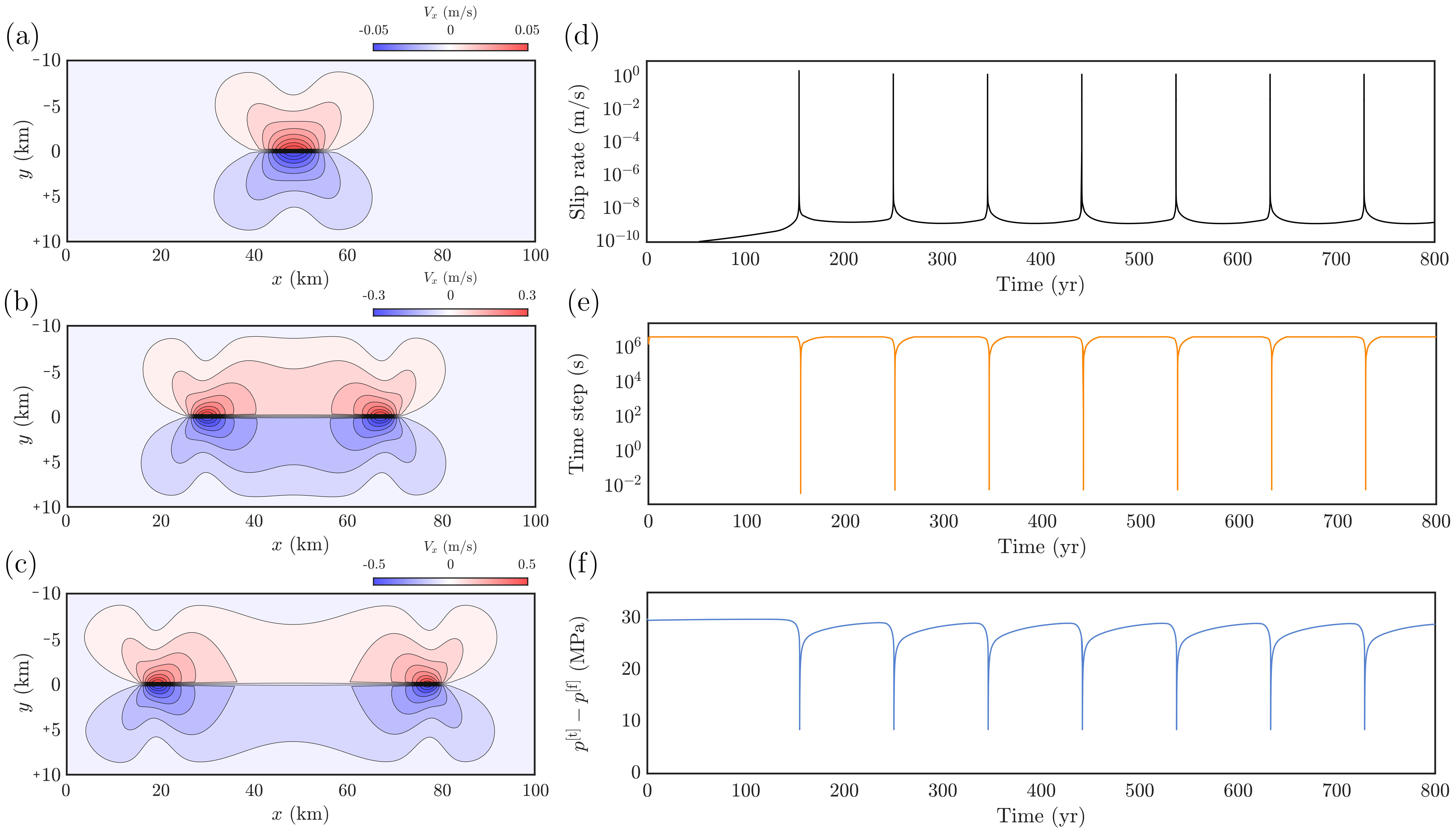

The model yields regular cycles of complete fault ruptures

Slip rate and the adaptive time-stepping vary by several orders of magnitude, from ~cm/yr to ~m/s, and from years to milliseconds

Pore-fluid pressure cycling on-fault varies by several MPa, while pore-pressure diffusion occurs over longer time scales

Coupling between viscoelasticity, pore-fluid pressure, and strain localization

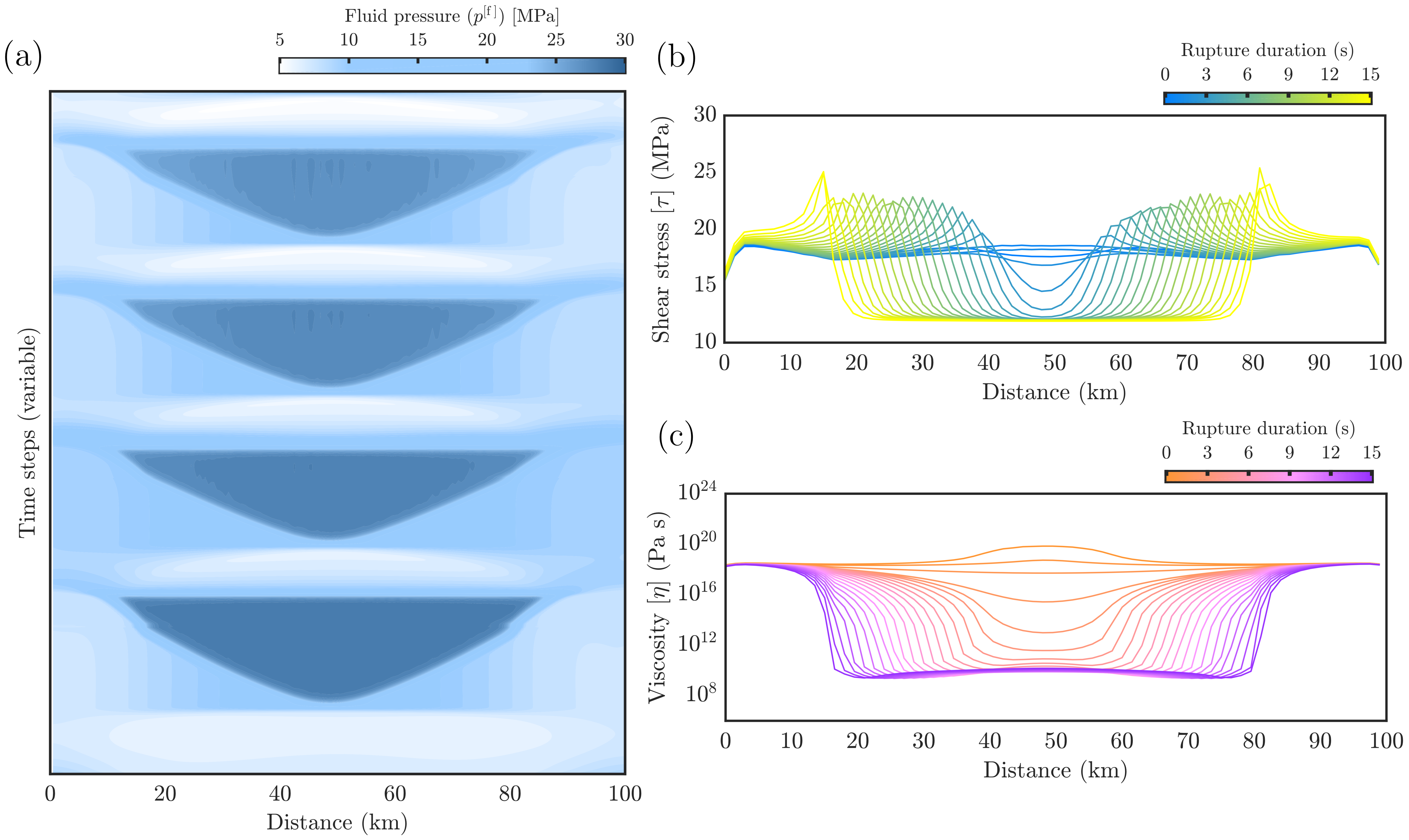

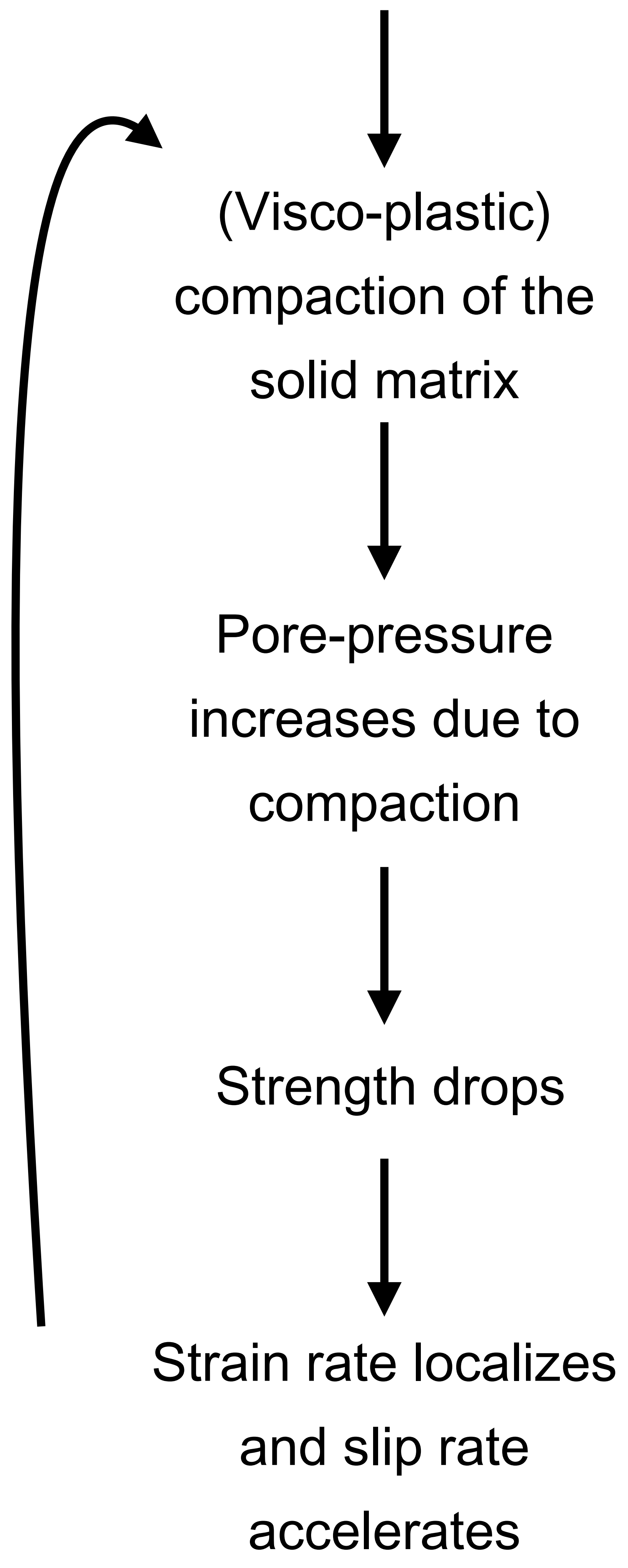

The initial pore-fluid pressure level affect the (a)seismic slip evolution

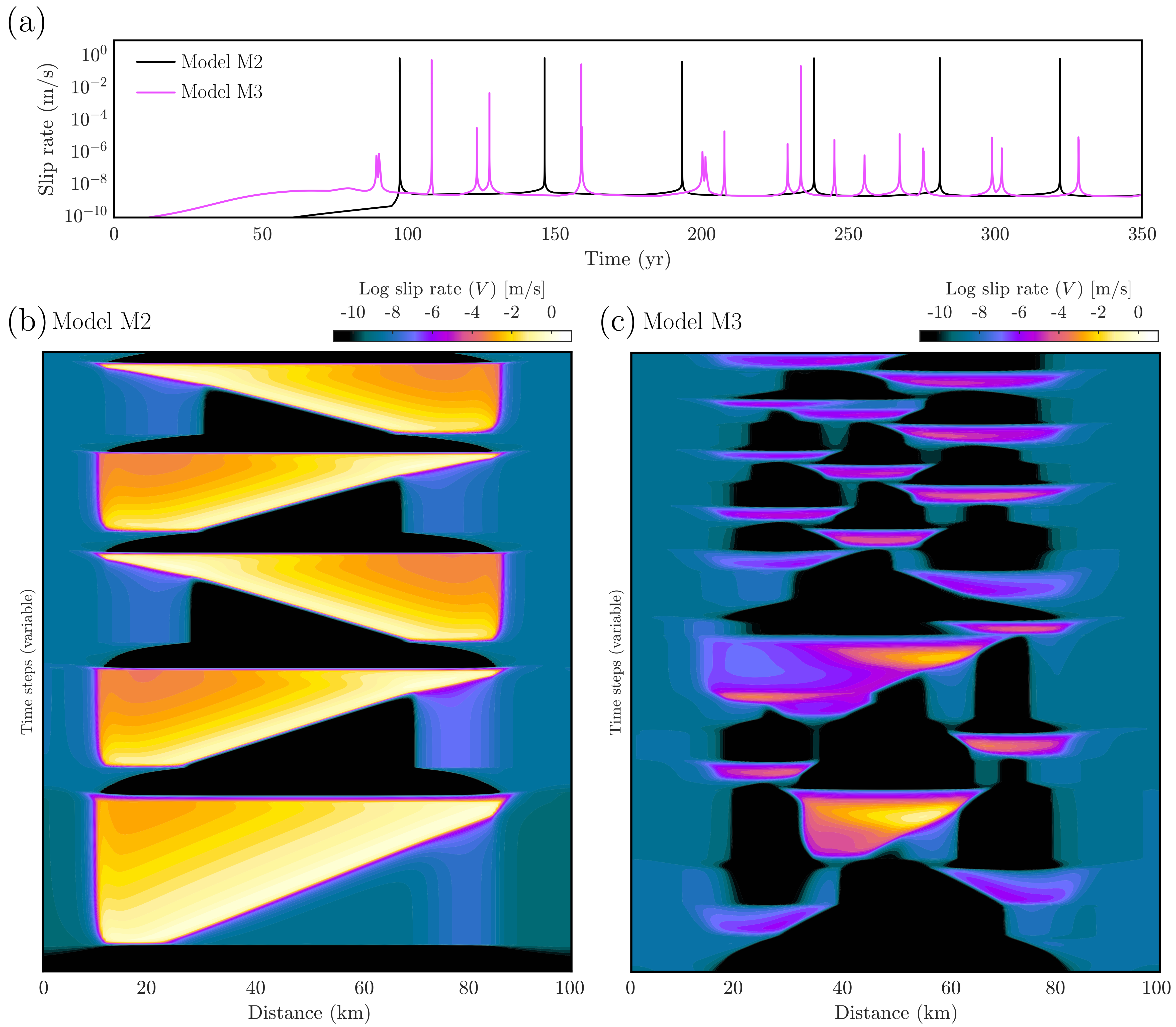

Model M2: lower power fluid pressure / higher effective pressure (40 MPa). Smaller nucleation size. As a results, events nucleation from the left or the right transition zones.

Model M3: higher power fluid pressure / lower effective pressure (10 MPa). Slow and fast slip events occurs depending on the local pore-fluid pressure.

Compaction/decompaction of the fault layer and propagation of a solitary porosity wave.

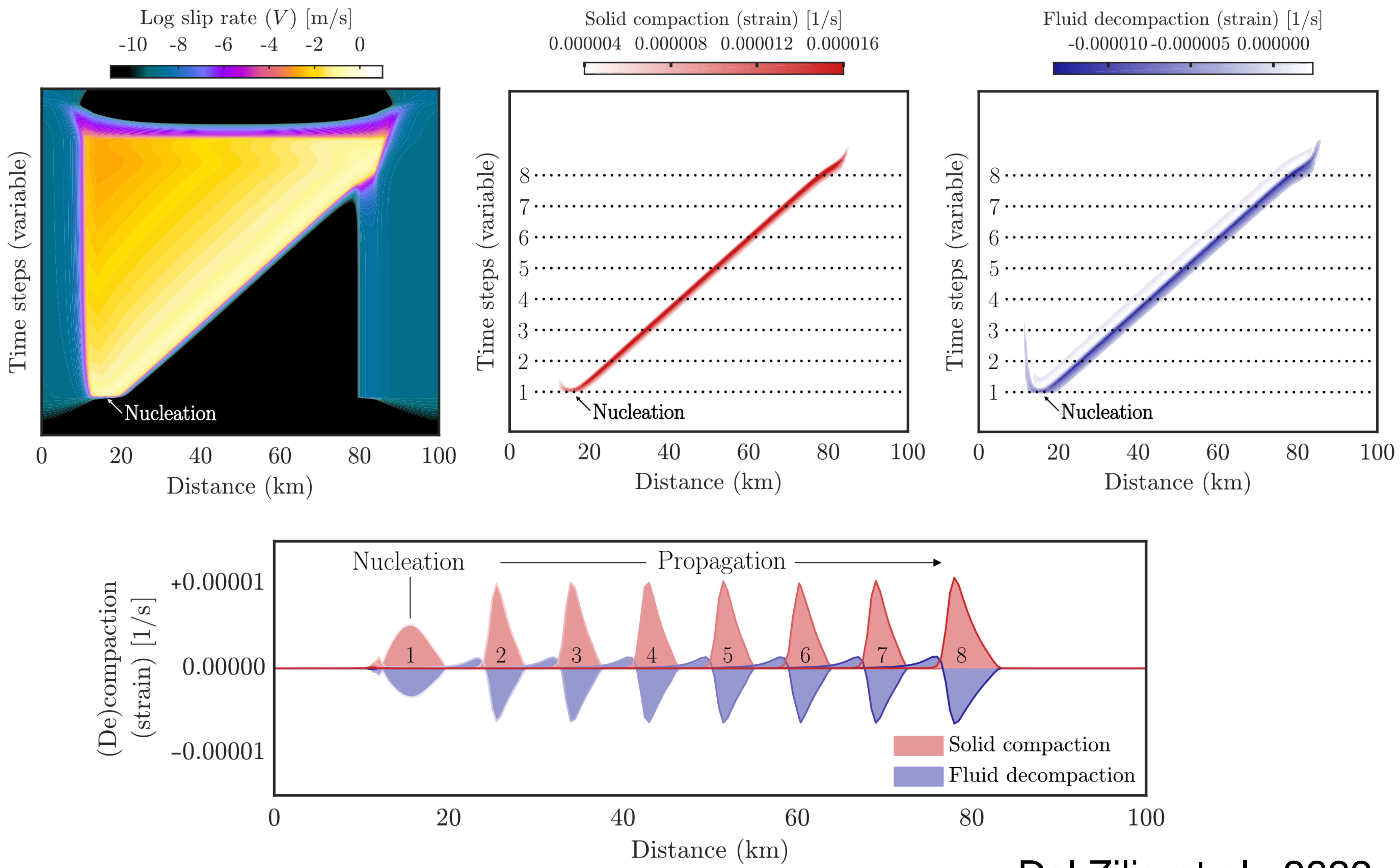

Dal Zilio et al., 2022

What is the solitary porosity wave? is a localized and self-sustaining disturbance or wave-like variation in porosity within a porous medium, such as a rock or soil, that maintains its shape and properties as it propagates through the medium.

These waves are often observed in geophysical and hydrogeological contexts and pressure changes, or mechanical deformation within the porous medium.

The role of fluids in seismic swarms

These experiments specifically investigate how the length of both permeability barriers (W_B) and pockets of high pore-fluid pressure (W_p) influence the propagation of slip patterns

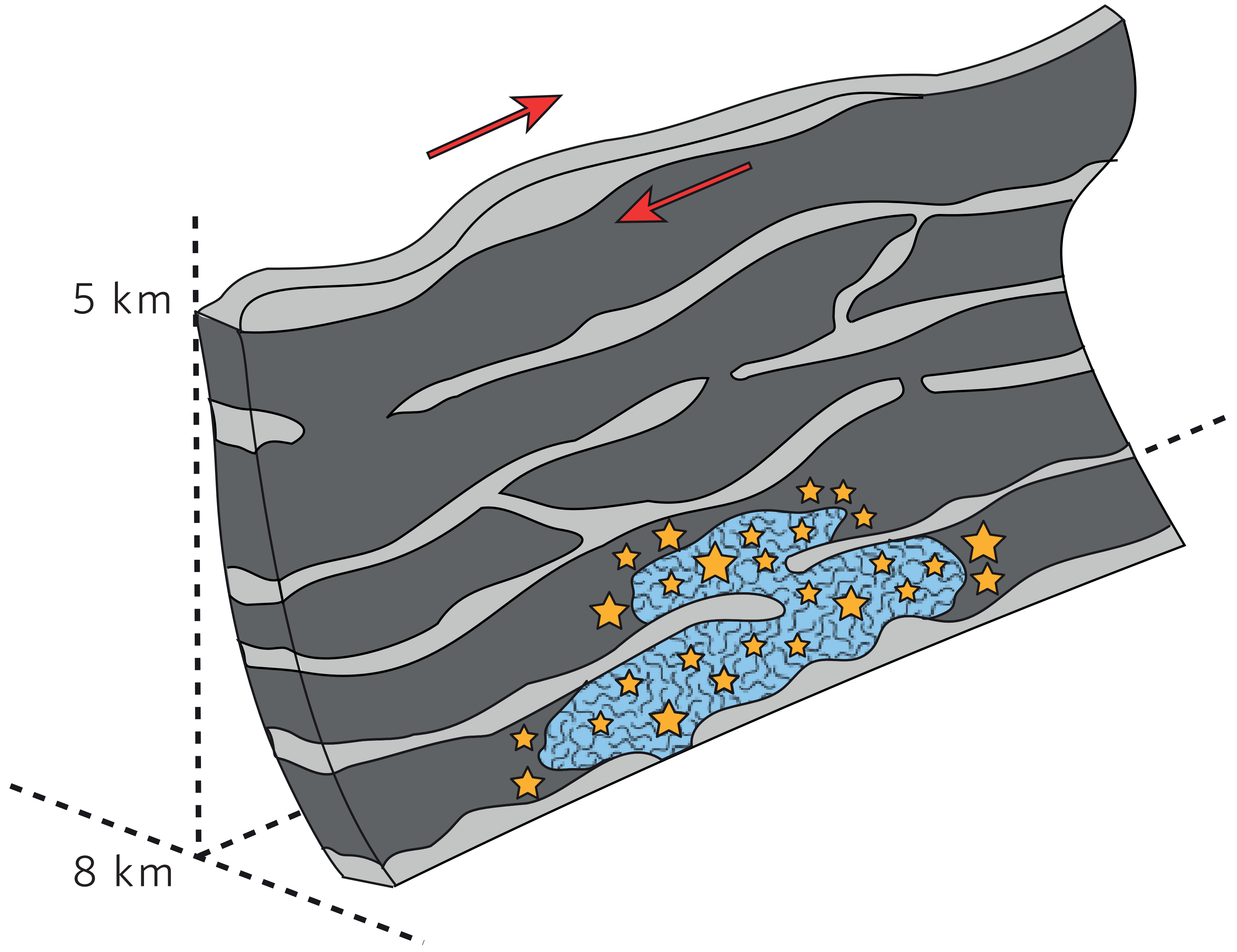

Ross et al., (2020)

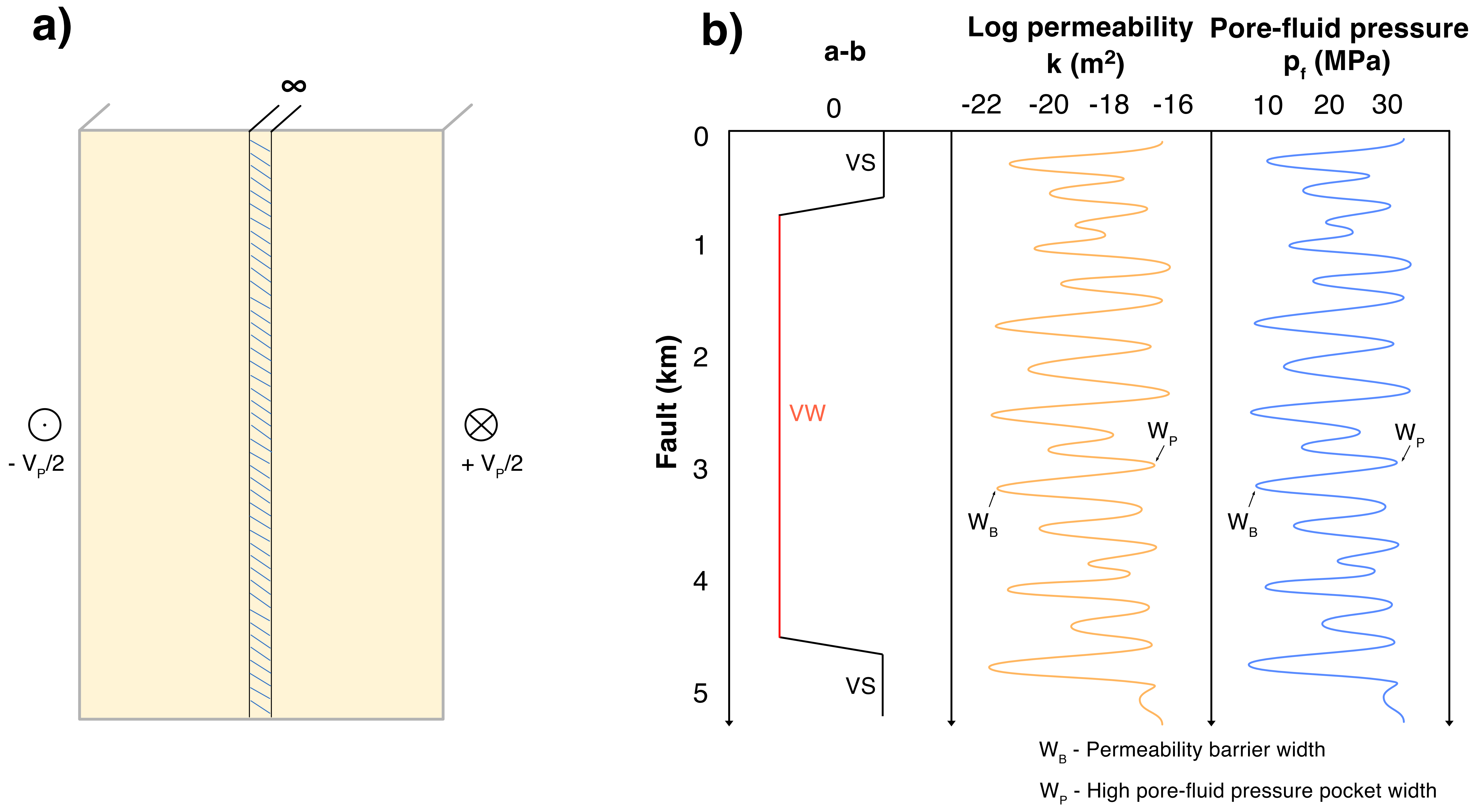

Key parameters include the ratio of permeability barrier to the nucleation size $W_B/h*$, and the ratio of high pore-fluid pressure pocket to the nucleation size $W_P/h*$, as they modulate the pore-fluid pressure.

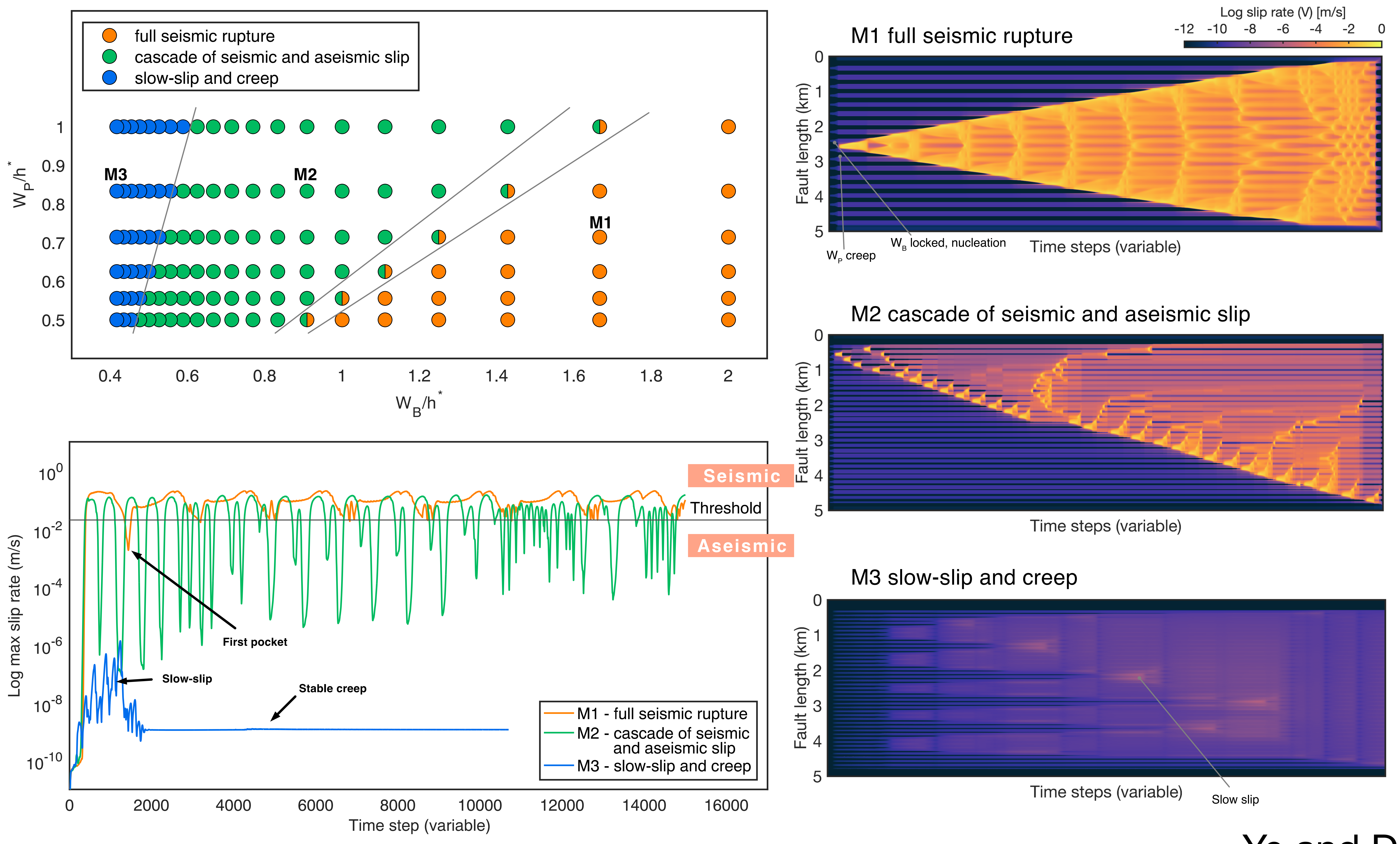

Ye and Dal Zilio (2023, in prep.)

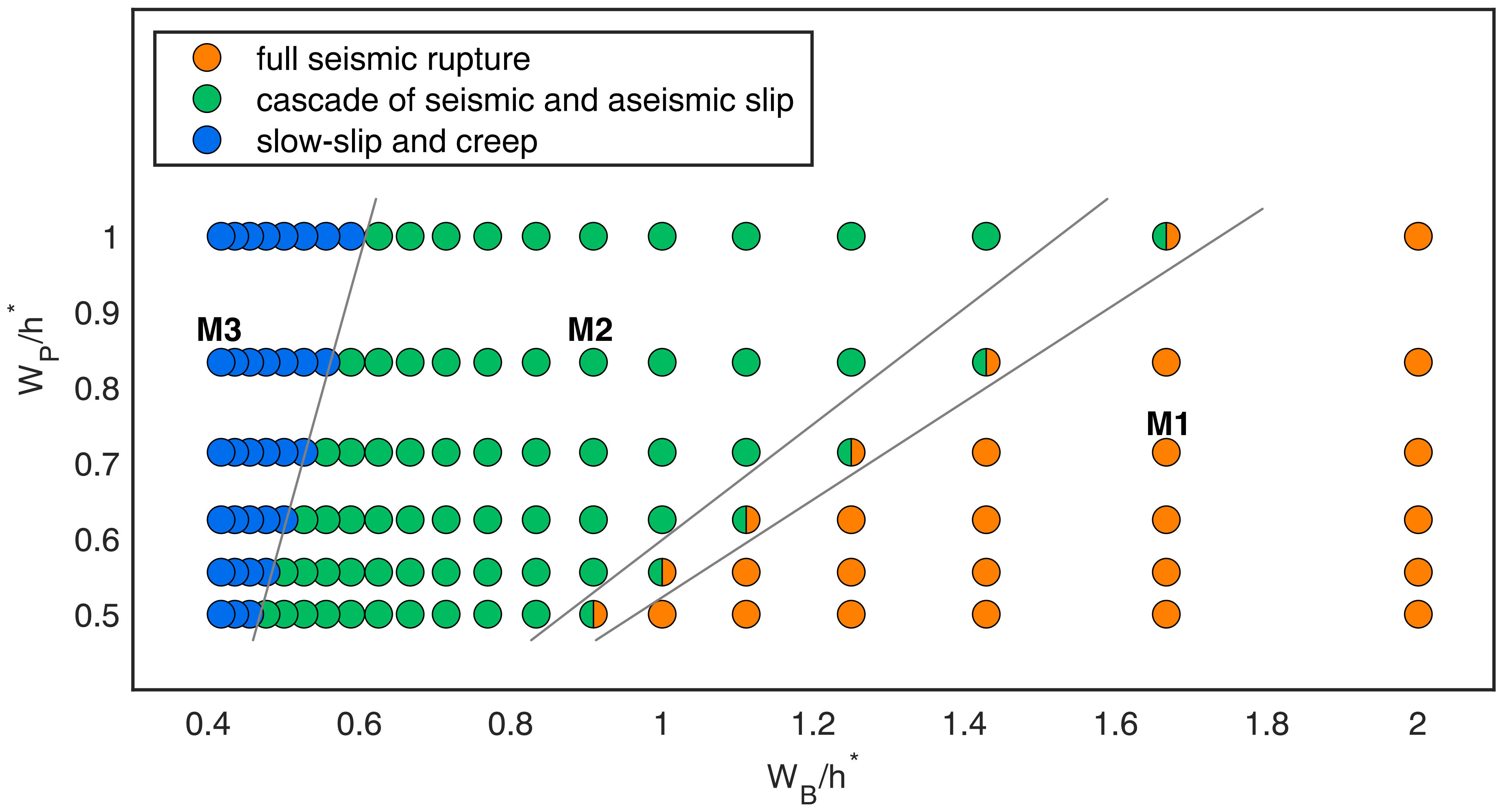

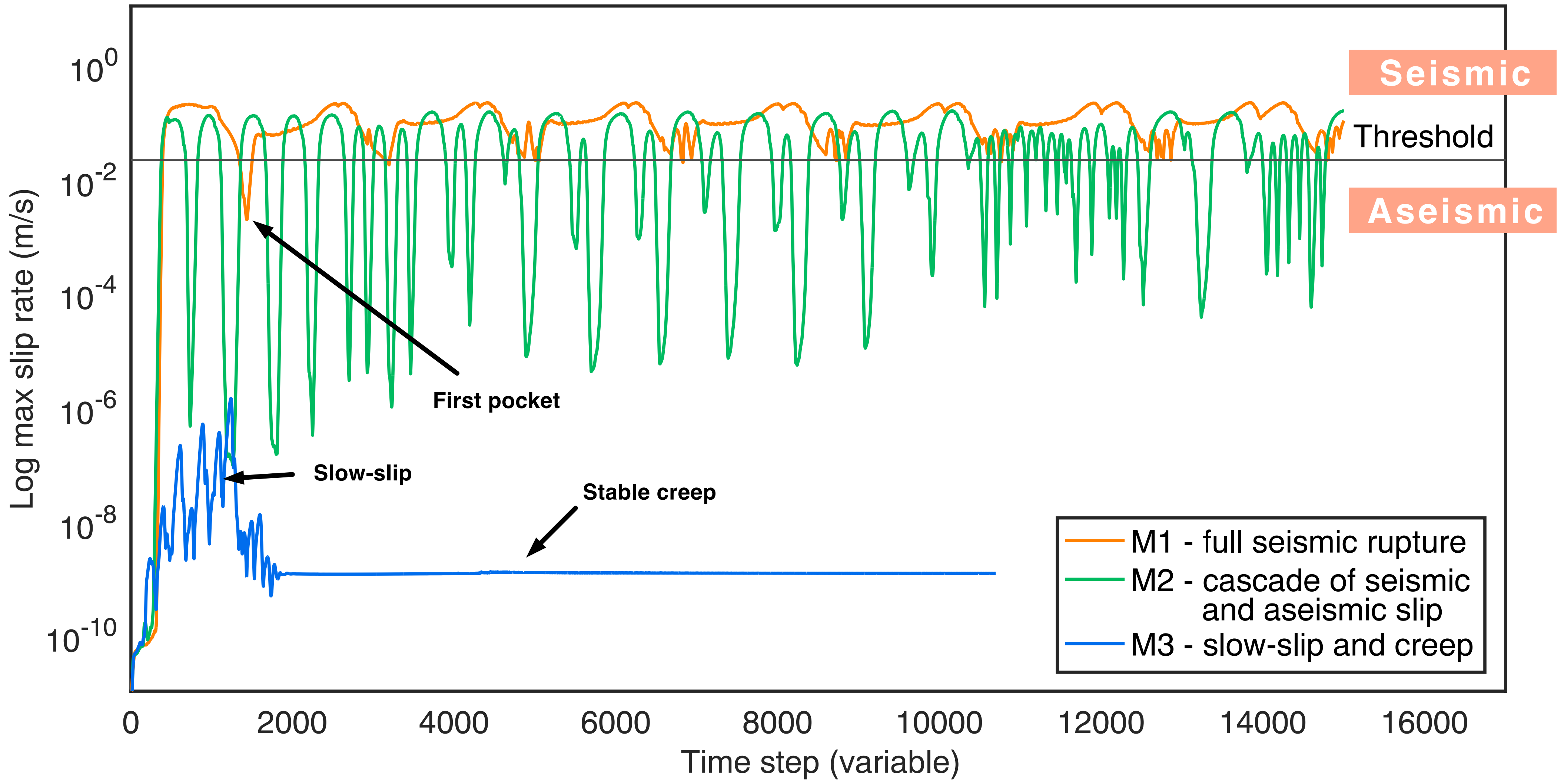

Results show that, while $W_p/h*$ remains between 0.5 and 1, an increase in $W_B/h*$ from 0.4 to 2 results in a transition from slow slip and aseismic creep to cascades of seismic and aseismic slip, ultimately leading to full seismic rupture.

This implies that an increase in size of permeability barriers facilitates fault instability and a switch from slow aseismic slip to dynamic rupture.

Ye and Dal Zilio (2023, in prep.)

Fault valving effects on faults

$$\frac{\partial k^*}{\partial t} = -\frac{V}{L}(k^* - k_{max}) - \frac{1}{T}(k^* - k_{min})$$

Permeability increases

Permeability decreases

Zhu et al., (2020)

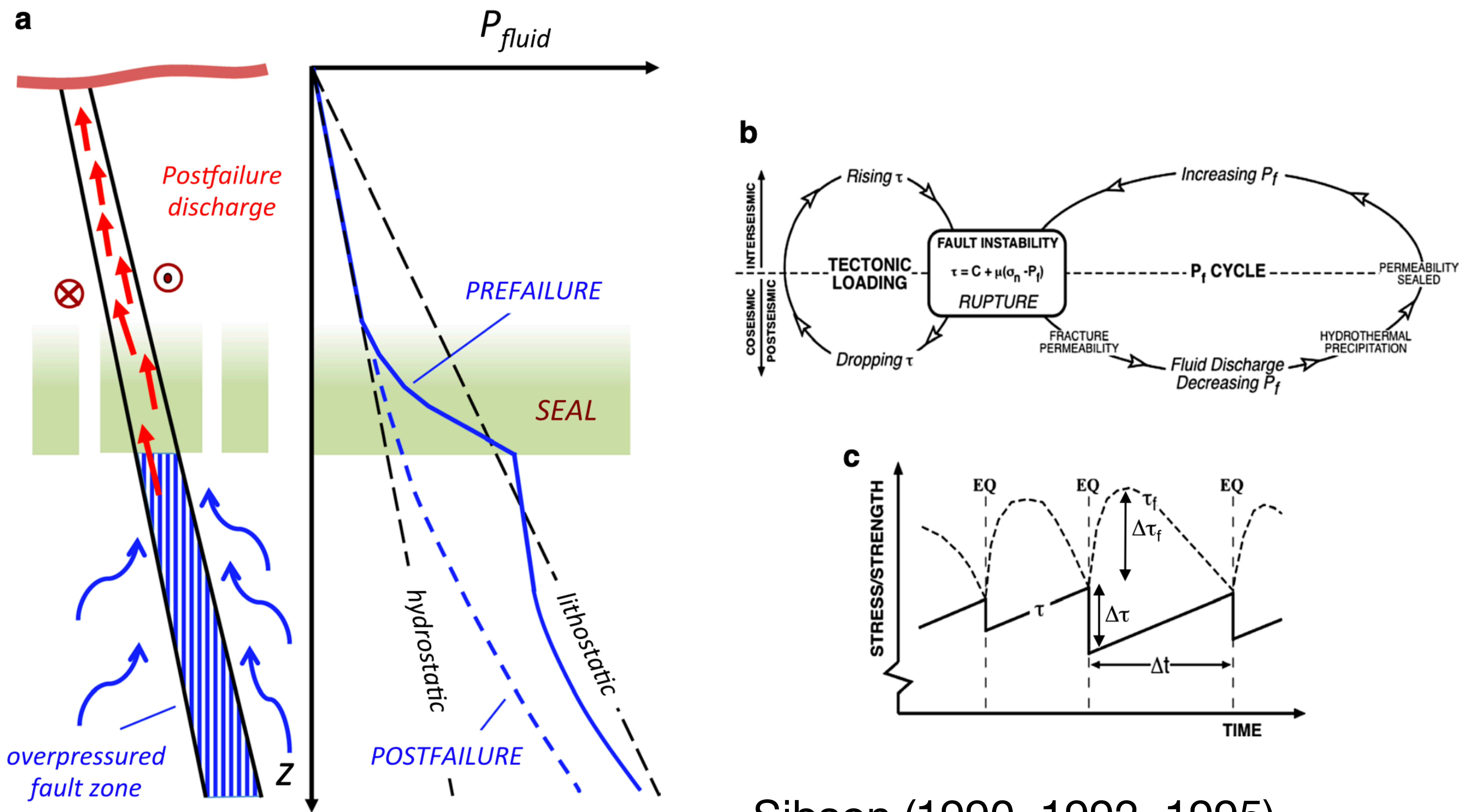

Sibson (1990, 1992, 1995)

Moderate permeability change

$k_{min} = 10^{-22}$ m^2 **$k_{max} = 10^{-15}$ m^2**

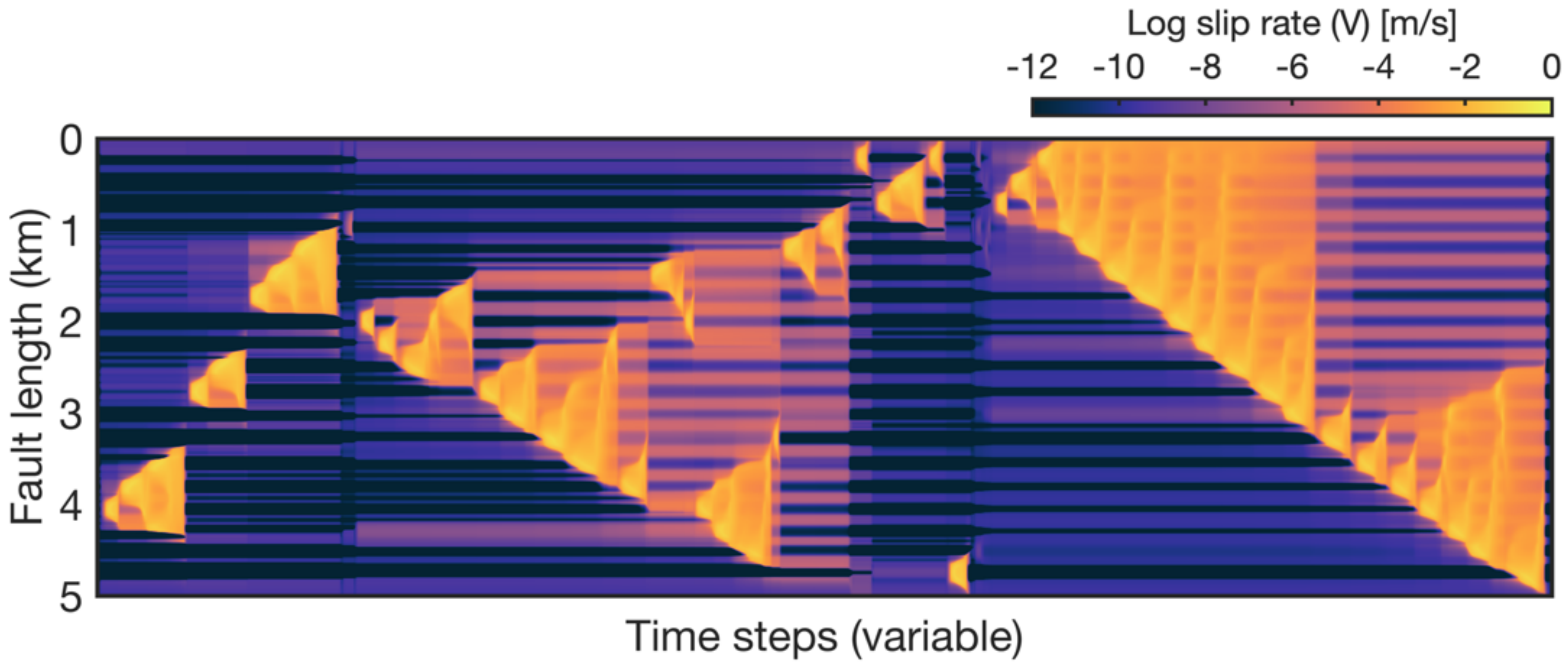

- **Slow** fluid pressure diffusion
- Slow propagation of **moderate/large** events

Strong permeability change

$k_{min} = 10^{-22}$ m^2 **$k_{max} = 10^{-12}$ m^2**

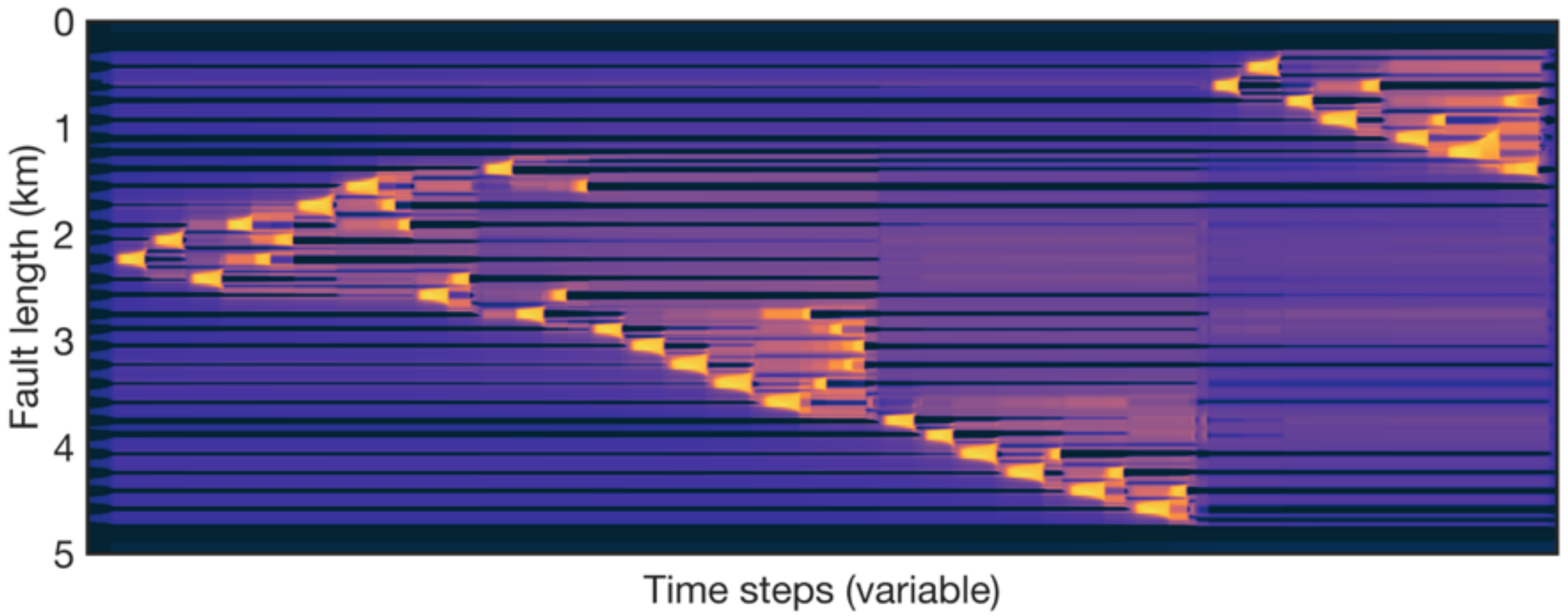

- **Fast** fluid pressure diffusion
- Rapid propagation of **small** events (swarms)

Results indicate that the rupture of sealed permeability barriers leads to the injection and redistribution of fluid through the fault zone. Pore-fluid pressure diffusion can rapidly propagate swarms and occasionally initiate a complete fault rupture.

Ye and Dal Zilio (2023, in prep.)

Depth-varying slip behaviour in subduction zones

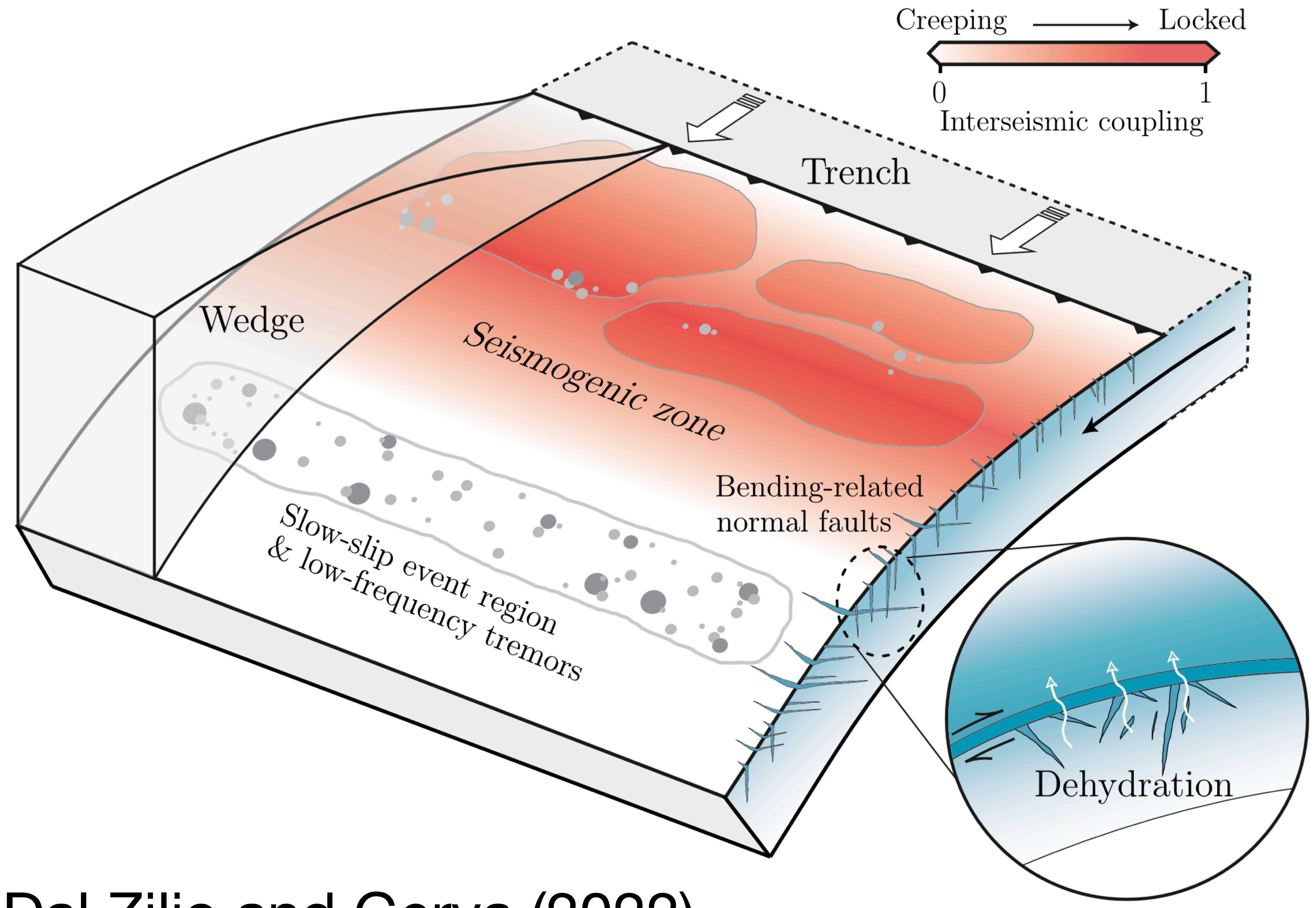

Dal Zilio and Gerya (2022)

In subduction zones, fluids are often invoked to explain slip processes on the megathrust, from great earthquakes to slow-slip events and tectonic tremors.

However, it is unclear how the transient evolution of pore-fluid is controlled by depth-dependent variations in hydraulic properties over a broad range of timescales concomitant with the full spectrum of seismic and aseismic slip.

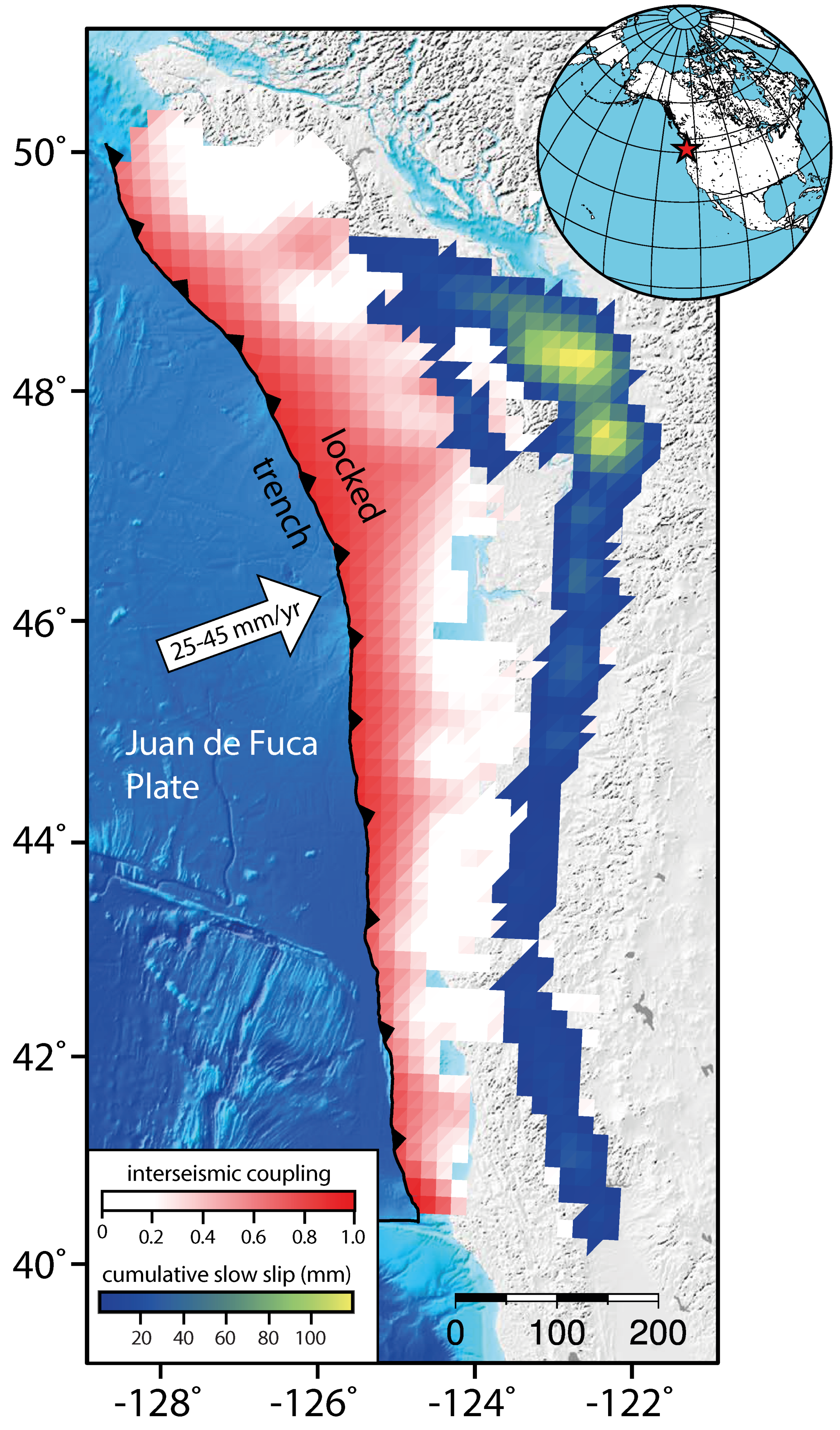

Michel, Gualandi, Avouac (2019a,b)

Depth-varying slip behaviour in subduction zones

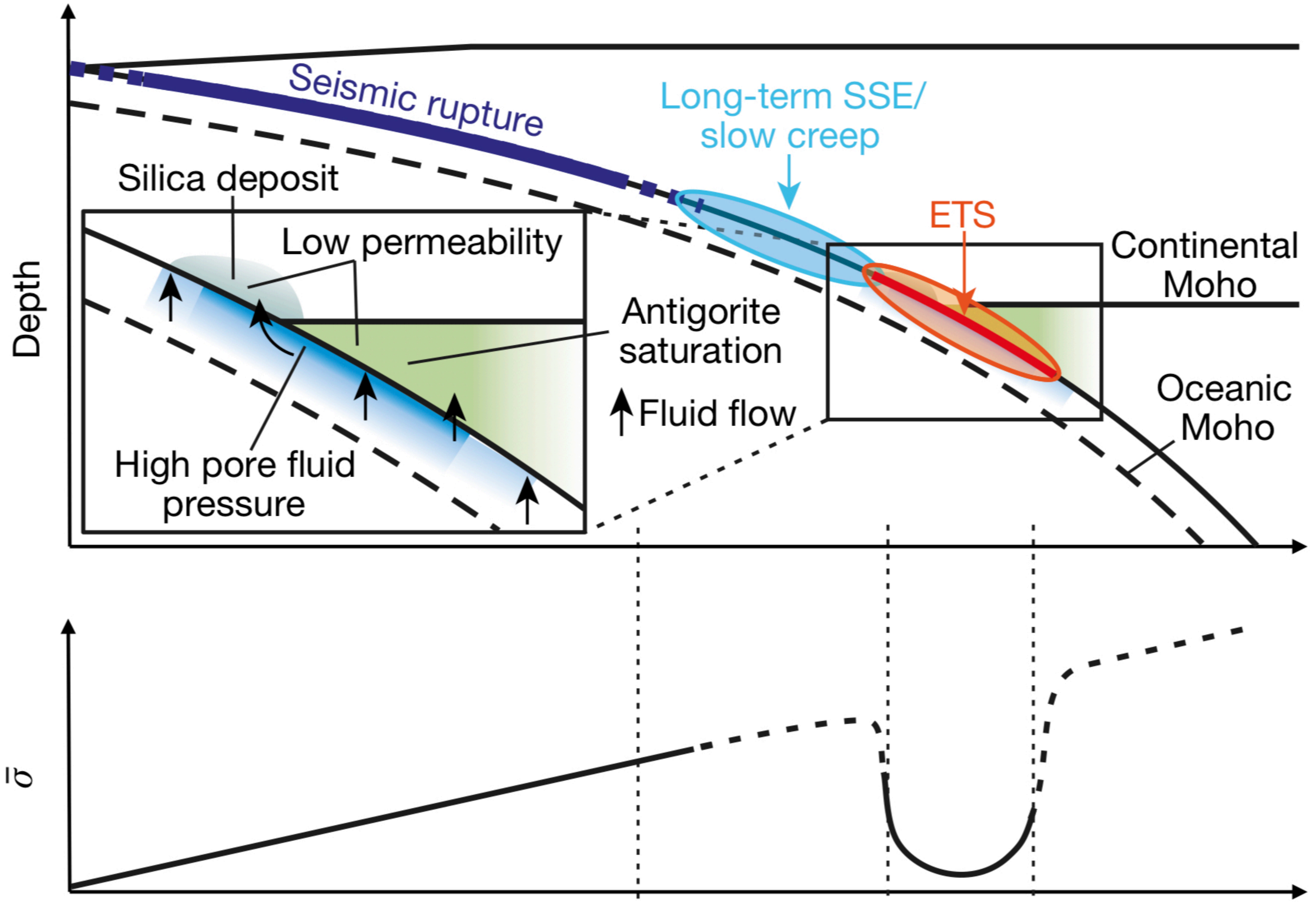

Gao and Wang (2017)

Several studies suggest that the megathrust permeability decreases with depth for a number of reasons: (1) volumetric expansion due to serpentinization (Kawano et al., 2011), which reduces grain boundary connectivity and, in turn, permeability; (2) large deposits of silica (SiO2) from slab-derived fluids (Audet and Bürgmann, 2014); and (3) stacking of relict shear zones atop the active plate boundary (Delph et al., 2021).

Depth-varying slip behaviour in subduction zones

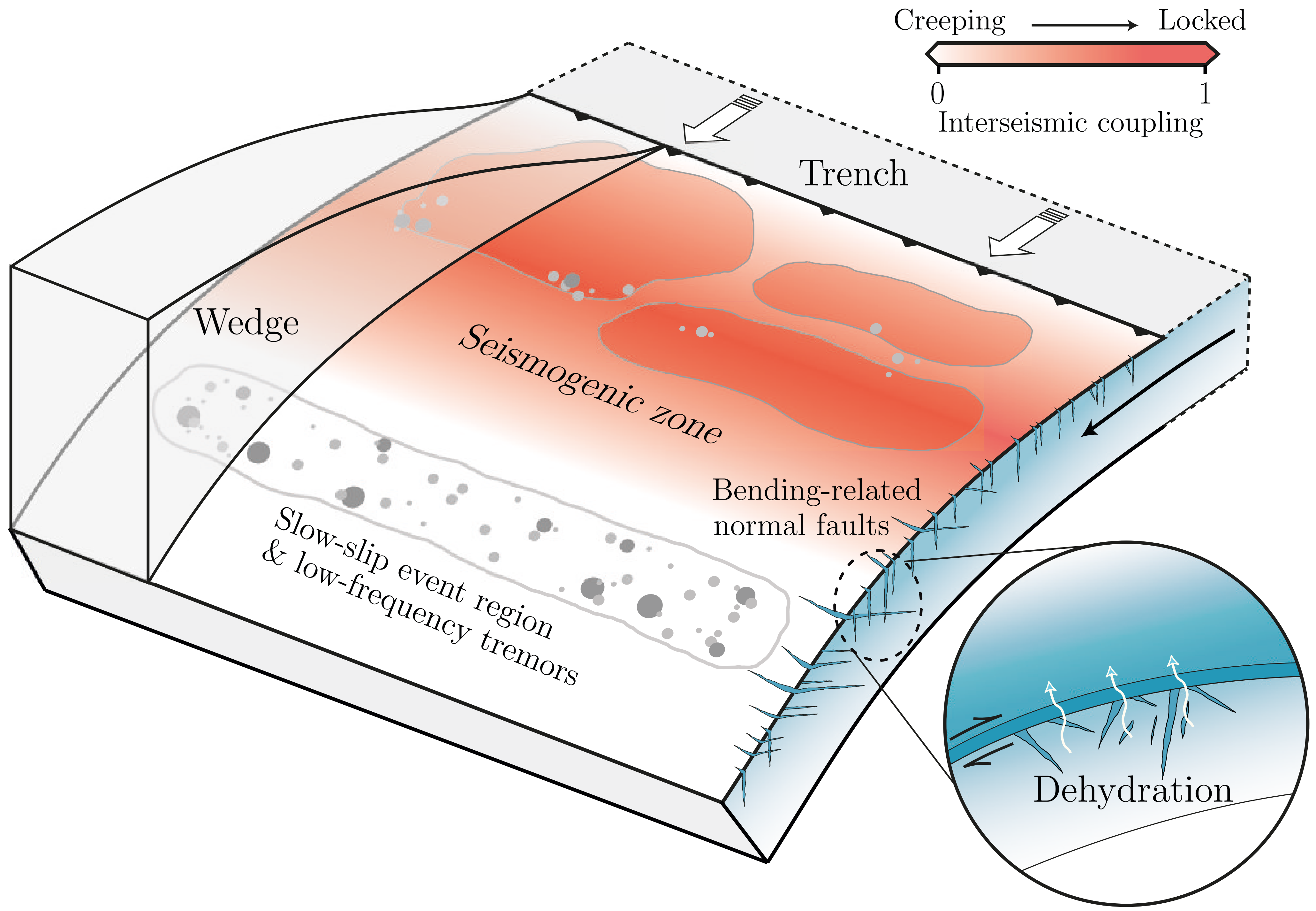

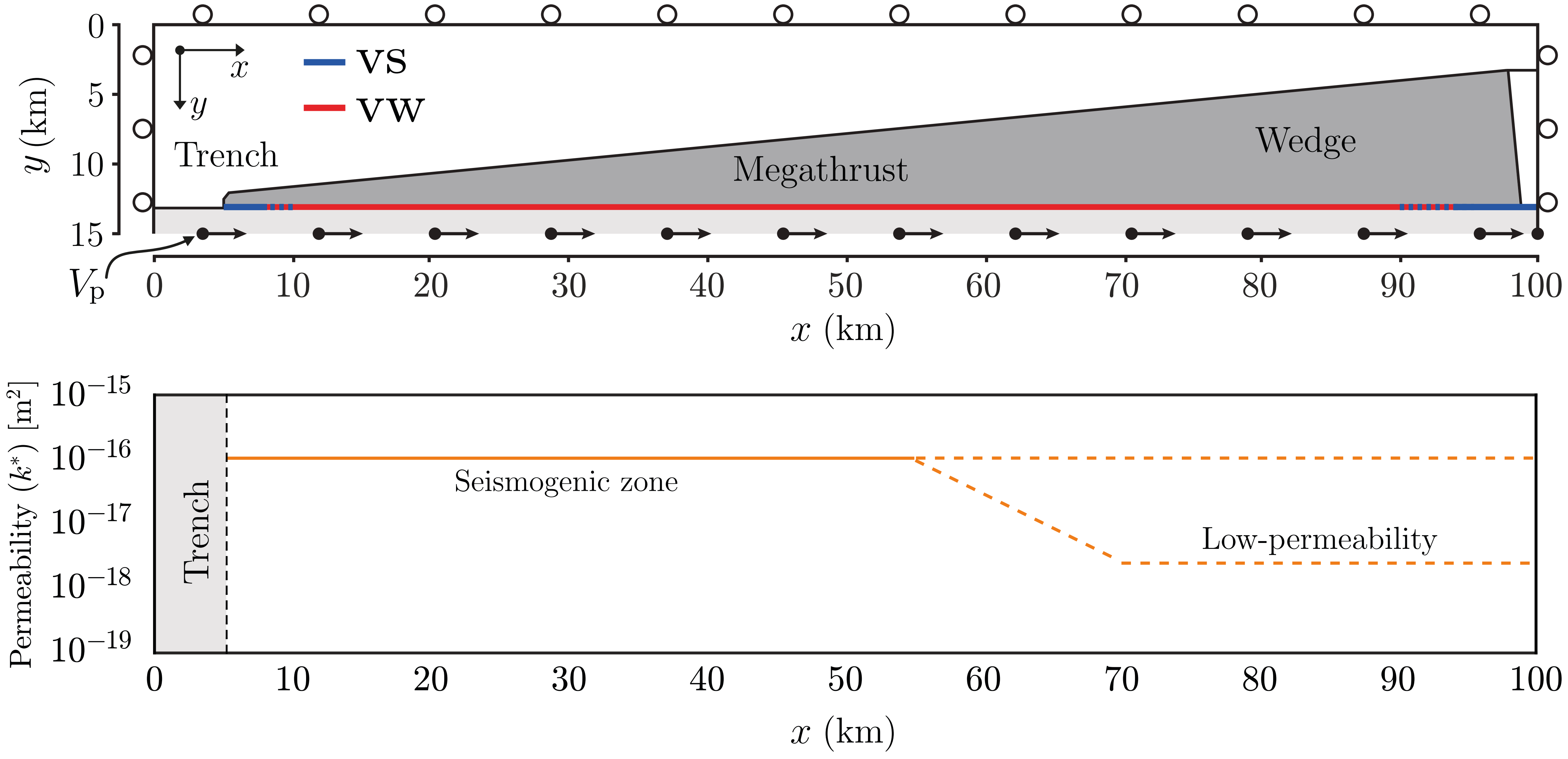

Dal Zilio and Gerya, 2022

Hydro-mechanical earthquake cycles in subduction zones

Model #1: homogeneous hydraulic properties

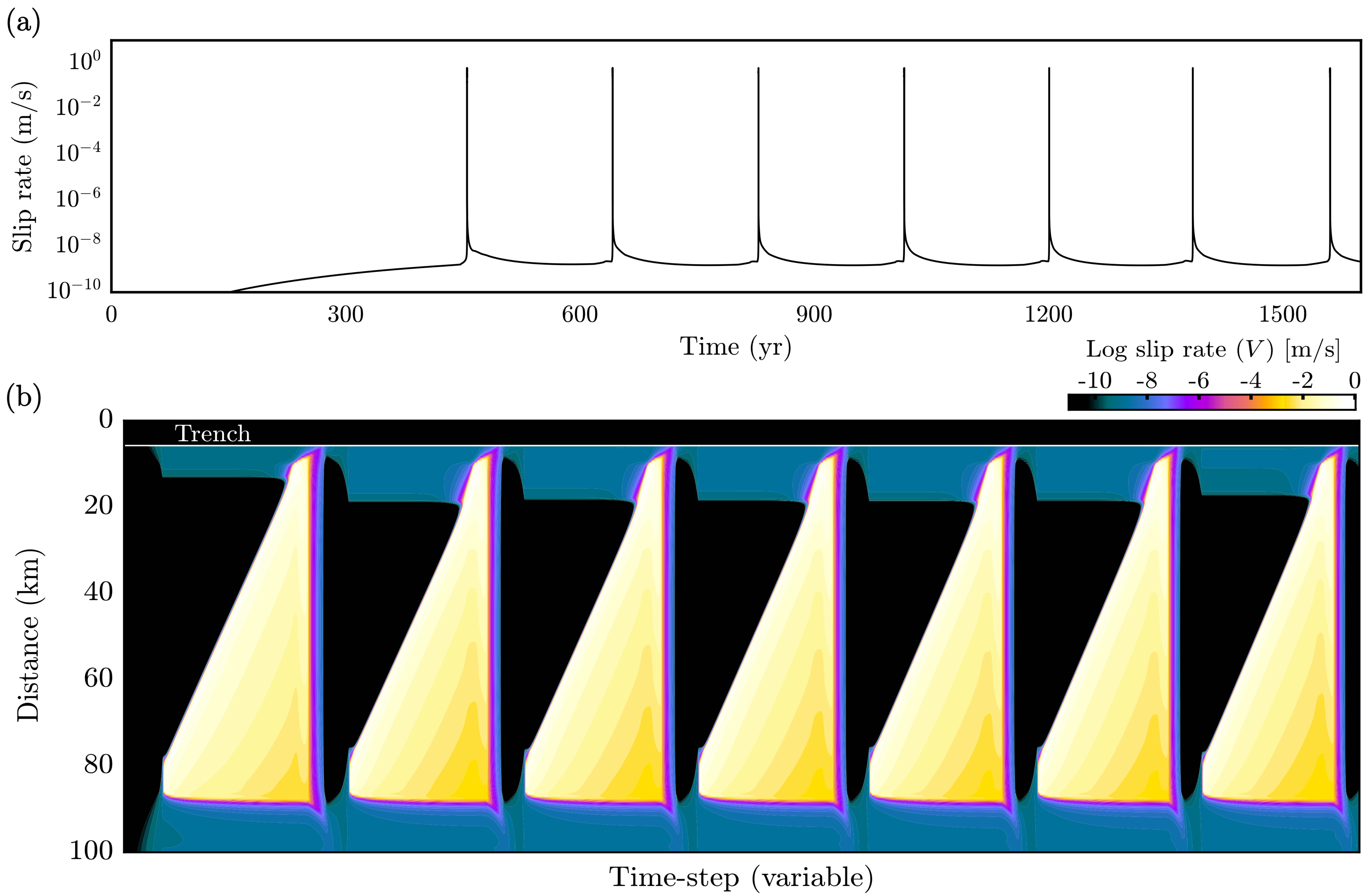

Given the constant and homogeneous hydraulic properties on the fault, the long-term fault behaviour shows similar features of earthquake recurrence and interseismic periods.

Dal Zilio and Gerya (2022)

Hydro-mechanical earthquake cycles in subduction zones

Model #2: Depth-varying permeability on-fault

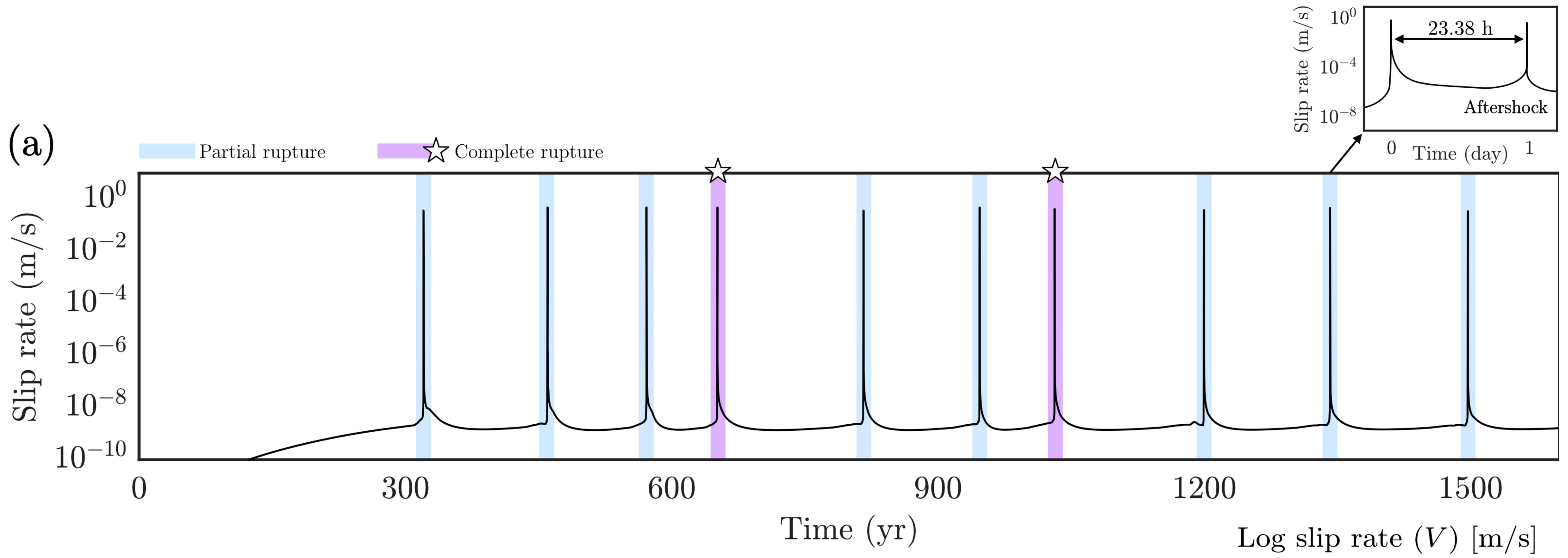

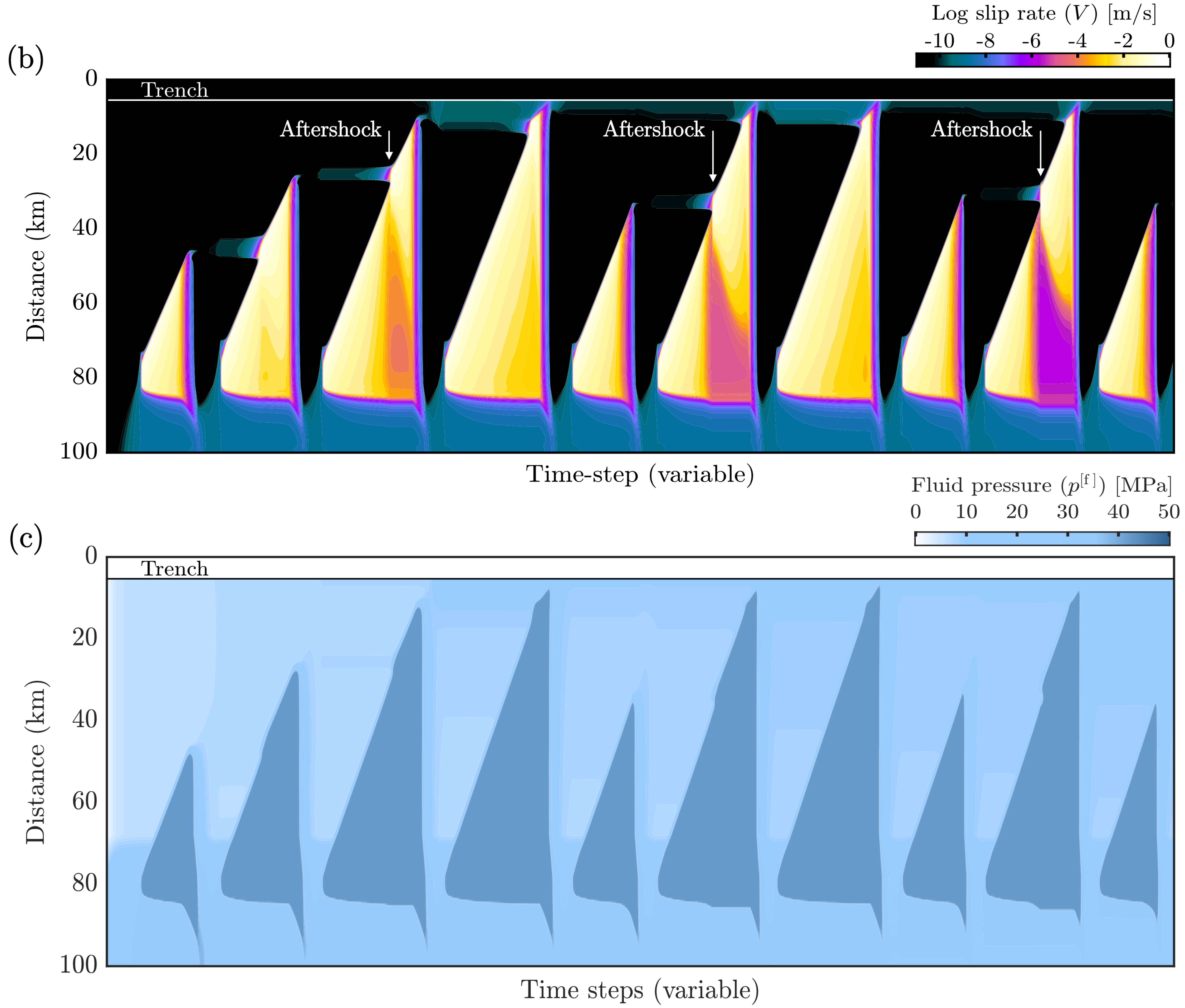

Modeling results indicate that the presence of a **low-permeability zone reduces fluid mobility** — particularly in the downdip edge of the fault where most of the seismic events nucleate.

Notably, the premature nucleation of seismic ruptures fuels the **emergence of partial and complete ruptures** on the megathrust, as well as shallow aftershocks.

Dal Zilio and Gerya (2022)